THE ASTRONOMICAL JOURNAL, 116:1816–1841, 1998 October

CIRCUMSTELLAR DISKS IN THE ORION NEBULA CLUSTER

LYNNE A. HILLENBRAND[1]
Department of Astronomy, California Institute of Technology, MS 105-24, Pasadena, CA 91125
STEPHEN E. STROM
Department of Astronomy, University of Massachusetts, LGRC 517G, Amherst, MA 01003
NURIA CALVET
Harvard-Smithsonian Center for Astrophysics, 60 Garden Street, Cambridge, MA 02138
K. MICHAEL MERRILL AND IAN GATLEY
Kitt Peak National Observatory, NOAO P.O. Box 26732, Tucson, AZ 85726-6732
AND
RUSSELL B. MAKIDON, MICHAEL R. MEYER, AND MICHAEL F. SKRUTSKIE
Department of Astronomy, University of Massachusetts, LGRC 517G, Amherst, MA 01003
Received 1998 February 3; revised 1998 May 27

ABSTRACT

We combine our previous optical spectroscopic and photometric analysis of ~1600 stars located in the Orion Nebula Cluster (ONC) with our own and published near-infrared photometric surveys of the region in order to investigate the evidence for and properties of circumstellar disks. We use the near-infrared continuum excess as our primary disk diagnostic, although we also study sources with Ca II triplet emission and those designated as "proplyds." The measured near-infrared excess is influenced by (1) the presence or absence of a circumstellar disk, (2) the relative importance of disk accretion and inner disk holes, (3) the relative contrast between photospheric and disk emission, and (4) system inclination. After attempting to understand the effects of these influences, we estimate the frequency of circumstellar disks and discuss the evidence for trends in the disk frequency with stellar mass (over the mass range <0.1–50 $M_\odot$), stellar age (over the age range <0.1–2 Myr), and projected cluster radius (over the radial range 0–3 pc). We find that the fraction of stars retaining their inner (<0.1 AU) circumstellar disks to the present time is at least 55% and probably no more than 90%, averaged over the entire range in stellar mass and stellar age represented in the ONC and over the entire area of our survey. We find no trend in the disk fraction with stellar age, at least not over the limited age range of the cluster. We find that more massive stars are less likely to have disks, consistent with a scenario in which the evolutionary timescales are more rapid for disks surrounding more massive stars than for disks surrounding less massive stars. We also find that the disk frequency begins to decrease toward the lowest masses, although objects of all masses (including those that appear to be substellar) can have disks. We find that the disk frequency increases toward the cluster center. We then argue, using several lines of evidence, that a large fraction of the disks associated with stars in the ONC are accretion disks. The observed trends with stellar age, stellar mass, and projected cluster radius in the disk frequency may, in fact, be driven primarily by trends in the disk accretion properties. From the magnitude of the near-infrared excess above that expected from pure irradiation disks, we find an accretion disk fraction among the stars identified as having disks of 61%–88%. In addition, approximately 20% of the stars in our optical spectroscopic sample show broad (several hundred km s^{-1} FWHM) Ca II emission lines, which are features often associated with accretion disk/wind phenomena; another 50% of the sample have Ca II lines that (at our spectral resolution) are "filled in," indicating an independently derived accretion disk frequency of ~70%. Finally, we discuss the near-infrared and optical emission-line properties of that portion of our sample identified from *Hubble Space Telescope* imaging as having a dark silhouette or an externally ionized structure. This sample, proposed in the literature to have accretion disks, appears to be no different in terms of its stellar or circumstellar properties from the rest of the ONC population. The only feature distinguishing these objects from their ONC siblings thus may be their current (but short-lived) proximity to the massive stars near the cluster center.

Key words: galaxies: open clusters and associations — stars: circumstellar matter — stars: formation — stars: pre–main-sequence

1. INTRODUCTION

It is generally accepted that circumstellar disks are a common by-product of the star formation process. In addition to the role an active accretion disk may play in determining the final mass of a star, such disks are also thought to be the potential sites of planet formation. Among the outstanding questions regarding young star/disk systems are the relationships between disk survival times and parent star mass, between disk accretion rates and parent star mass/age, and between disk properties and the local environment (e.g., stellar density). Because of its complete sampling of the stellar mass spectrum (down to, and perhaps even below, the hydrogen burning limit; Hillenbrand 1997), its extreme youth ($\bar{\tau} < 1$ Myr;

[1] Work conducted at Department of Astronomy, University of California, 601 Campbell Hall, Berkeley, CA 94720; lah@warning.caltech.edu.

Hillenbrand 1997; Herbig & Terndrup 1986), and its high stellar density ($\rho_0 \approx 2 \times 10^4$ stars pc^{-3}; Hillenbrand & Hartmann 1998; McCaughrean & Stauffer 1994), the Orion Nebula Cluster (ONC) affords us the opportunity to address these questions for a statistically significant population of stars. The ONC contains $\sim$1600 optically visible stars (Hillenbrand 1997) within a projected radius of 2.5 pc from the Trapezium stars, and at least 120% more objects (Hillenbrand et al. 1999) within that projected radius, which are still embedded within the optically opaque remains of the molecular cloud that gave birth to the stellar cluster. The ONC is the nearest ($d \approx 470$ pc; Genzel et al. 1981; Walker 1969) example of the dense, rich clusters that are thought to be producing the majority of stars currently forming in the Milky Way. Thus detailed understanding of the young stellar population emerging from such a region may provide insight into the factors controlling the formation, early evolution, and initial distribution of stellar properties (e.g., masses and angular momenta) among "typical" stars in the Galaxy.

In Hillenbrand (1997) we assembled an optical photometric and spectroscopic database and discussed the distributions of stellar masses and ages as derived from a theoretical H-R diagram. In this paper we assemble an infrared photometric data set that, in combination with the optical database, enables measurement of near-infrared continuum emission arising from circumstellar (accretion) disks. Specifically, we can (1) search for disk signatures for young stars spanning a range in mass $\lesssim 0.1 - 50\ M_\odot$ and age $\lesssim$0.1–2 Myr, (2) compare the distribution of stellar masses among stars surrounded by disks and those that lack disks, (3) constrain disk lifetimes as a function of stellar mass, and (4) discuss the correlations between location within the ONC and disk frequency, in order to understand the effects of environment on disk evolution. The infrared data set also enables discussion of the optically invisible stellar population, which we defer to a later paper.

In § 2 we present the infrared (primarily *JHK*) photometry and quantify the limits of the infrared surveys. In § 3.1 we discuss near-infrared continuum excesses as diagnosed via $I_C - K$ colors that have been corrected for the effects of foreground extinction and from which the underlying stellar photosphere has been subtracted. In § 3.2 we discuss our sensitivity to the detection of disks of different accretion rate, inclination, and inner disk hole size surrounding stars of different mass and age. In § 4 we present the measured near-infrared excesses in comparison with the theoretical expectations; the presence of near-infrared emission above the value expected from a young stellar photosphere is interpreted as arising in a circumstellar disk. In § 5 we describe our methodology for estimating the frequency of star/disk systems in the ONC. In § 6 we explore the relationships between disk frequency and stellar age, stellar mass, and position within the cluster. In § 7 we present evidence that a large majority of the ONC disks are probably accretion disks, based on (§ 7.1) near-infrared excess above the value expected from a pure-irradiation disk, (§ 7.2) Ca II triplet emission lines, and (§ 7.3) the 99 sources in our sample identified in the work of O'Dell & Wong (1996, and references therein) as being either externally ionized or seen in silhouette against the background of the bright emission nebula. In the Appendix we discuss the utility of various observed color-color diagrams in identifying stars with near-infrared excess.

2. INFRARED PHOTOMETRY

Optical + near-infrared imaging surveys provide the most efficient means for diagnosing the presence of circumstellar disks among large samples of pre–main-sequence stars, this via their ability to detect emission above photospheric levels due to dust and gas heated by a combination of irradiation and accretion. We have already assembled a large database of optical imaging photometry and optical spectroscopy for stars in the ONC. In this section, we discuss the components of an even larger database containing both new and existing near-infrared photometric measurements for more than $\sim$1400 optically visible sources and $\sim$2000 optically invisible sources.

2.1. *Data Acquired from the Literature*

First, a complete literature search for all infrared photometry of ONC stars was conducted. *JHK* and some limited *LNQ* photometry is available from (1) the imaging surveys of McCaughrean & Stauffer (1994) and McCaughrean & O'Dell (1996) covering approximately the central 1.5 × 1.5 arcmin^2 of the ONC, of Ali & Depoy (1995) over about 39 × 39 arcmin^2, of Jones et al. (1994), covering approximately 15 × 7 arcmin^2 centered on the OMC2 region, and of Hyland, Allen & Bailey (1993; as reported by Samuel 1993), covering about 13 × 14 arcmin^2; and (2) the single channel photometer measurements of Rydgren & Vrba (1984), Breger, Gehrz, & Hackwell (1981), Smith (1976), McNamara (1976), Penston, Hunter, & O'Neill (1975), Penston (1973), Ney, Strecker, & Gehrz (1973), and Lee (1968).

2.2. *New Observations*

New *JHK* data were obtained (1) by Hillenbrand & Strom in 1991 November and December with the OTTO photometer (Gillett & Joyce 1975), mounted on the KPNO 50″ telescope, for proper motion members brighter than $B = 13$ over several degrees of the Orion association (with 47 stars located within the $r_{\rm projected} < 2.5$ pc region considered in this paper); (2) by Merrill & Gatley in 1991 with the SQIID camera (Ellis et al. 1992), at the KPNO 50″, over about 30 × 45 arcmin^2 of the ONC with a plate scale of 1.3 arcsec pixel^{-1}; (3) by Hillenbrand & Meyer in 1993 March with the UMass NICMASS camera (see references in Joyce et al. 1998), at the MDM 1.3 m telescope, over the inner 3.5 × 3.5 arcmin^2 of the ONC with a plate scale of 0.8 arcsec pixel^{-1}.

The OTTO data were taken using a standard source-sky–sky-source beam switching pattern through a 15″ beam with a 30″ throw. Calibration was performed using the standards of Elias et al. (1982), thus placing the data on the CIT photometric system (within color terms of an order of 5%; Kenyon 1988). For the imaging data, see Hillenbrand et al. (1993) for a generic description of the SQIID image processing and Hillenbrand et al. (1995) for a generic description of the NICMASS image processing. Photometry was extracted from the processed images separately by Makidon and by Hillenbrand through apertures 6–12 pixels in diameter. Each object was examined by eye to identify various sources of error related to the extreme crowding in this region, and stars whose photometry was deemed questionable were removed. The maximum tolerated measurement error, as calculated from source photon statistics and determination of sky, was 0.2 mag: the mean error with magnitude is (0.008, 0.015, 0.035, 0.07, 0.20) for

$J = (12, 13, 14, 15, 16)$; (0.005, 0.01, 0.03, 0.08, 0.18) for $H = (11, 12, 13, 14, 15)$; and (0.01, 0.02, 0.04, 0.08, 0.15) for $K = (10, 11, 12, 13, 14)$. All photometry was calibrated by bootstrapping the OTTO measurements.

The integrity of the new JHK photometry was studied via comparison with all previous measurements referenced above. Histograms of magnitude differences between our and previous photometry show a two-component Gaussian structure centered at 0 mag, with a strong, narrow component of width $\sigma \approx 0.05$ mag at each of K, H, J and a weak, broad component of width $\sigma = 0.19$ mag at K, $\sigma = 0.16$ mag at H, and $\sigma = 0.18$ mag at J. We interpret the narrow component to reflect typical measurement errors. The broad, shallow component exceeds the measurement errors but is consistent with the known infrared variability of several tenths of a magnitude for stars in this region (M. F. Skrutskie, unpublished data). Histograms of the $J-H$ and $H-K$ color differences have Gaussian widths of 0.14 mag and 0.10 mag, respectively, and thus show smaller dispersion than is found for the magnitude differences.

2.3. *The Compiled Infrared Database*

The optical information presented in Hillenbrand (1997) was combined with all available infrared photometric information (our new photometry plus that from the literature) first by associating a K-band magnitude to every optical source and then adding in $H-K$ and $J-H$ colors as they were available. We prioritized the various sources of infrared data in the order of decreasing spatial resolution. For the K magnitudes, we used the McCaughrean & Stauffer measurements with first priority (72 stars), employing their cross identifications to match optical and infrared sources. With second priority, we used our own NICMASS measurements for 84 stars of 89 measured, our own SQIID measurements for 941 of 1022 measured, and our own OTTO measurements for 15 stars of 47 measured. We used the Ali & Depoy magnitudes with third priority (213 stars); their archived data set was transformed from equinox 1950 to 2000 and was merged with our optical sources by looking for positional matches within a 2.″0 search radius. A histogram of the absolute value of the positional offsets between the Ali & Depoy infrared mosaic positions and our optical positions peaks at 0.″9 with a half-width of 0.″5. Furthermore, the Ali & Depoy database contains a large number of duplicate sources, e.g., multiple positions quoted in their Table 2 that fall within 0.″5 of one another despite the 1.″5 plate scale of their images. In all of these cases, however, the photometric measurements are (nearly) identical and we could easily eliminate the duplicates. The Hyland, Allen, & Bailey measurements were used with fourth priority (11 stars), utilitizing their cross identifications and also adding a few newly discovered ones. Finally, the measurements of Jones et al. were used for 48 stars after finding positional matches via coordinates. About 10 other K magnitudes come from the older literature.

No attempt was made to place the K-band magnitudes of these different data sets on the same photometric system, since this would require knowledge of color terms that cannot be reconstructed from the information in the literature. We note, however, that comparison of the photometry for stars in common between this array of surveys showed remarkably low dispersion (0.05–0.2 mag) given the different observational techniques, the complexity of the region, and the intrinsic source variability.

In summary, unique infrared counterparts were found for 88% (1394/1578) of the optical sources, with 70% (1101) having full JHK data and 52% (813) having stellar masses and ages derived from the H-R diagram. Conversely, optical counterparts were found for less than 50% of all infrared sources projected within ~ 2.5 pc of the ONC center identified to date. This suggests that while the near-infrared surveys certainly sample the stellar population associated with the ONC, they also probe an embedded population that may be located in the background molecular cloud. The compiled infrared database is given in Table 1. A histogram of K-band magnitudes is shown in Figure 1, with the distributions for optically visible and optically invisible stars shown in separate panels. We defer discussion of the optically invisible, embedded population of ~ 2000 stars to a subsequent paper (Hillenbrand et al. 1999).

In Figures 2, 3, and 4 we show the $(V-I_C)$-(I_C-K), $(V-I_C)$-$(H-K)$, and $(J-H)$-$(H-K)$ diagrams for the optically visible stars. These figures have been divided into bins of projected cluster radius for ease of presentation. Solid lines in each figure indicate the dwarf and giant loci, while dotted lines indicate reddening vectors. Consistent with the results of optical analysis of these stars (Hillenbrand 1997), the distribution of data points in Figures 2, 3, and 4 indicates a stellar population dominated by late-type stars with moderately low values of extinction. Furthermore, the distribution of data points also indicates a large fraction of stars (those that lie redward of the reddening vectors and thus cannot be dereddened such that they intersect the locus of normal photospheric colors) to have near-infrared excesses. Both the magnitude of the near-infrared excesses and the fraction of stars in each panel showing near-infrared excesses appears to be higher at smaller projected cluster radii. However, it is possible for a star to lie within the reddening vectors yet have a small amount of near-infrared excess. In this paper we individually deredden the stars in these color-color diagrams and then subtract from the remaining color the contribution of the stellar photosphere. The remaining color excess is attributed to circumstellar dust. This procedure allows us to investigate near-infrared

TABLE 1

INFRARED AND EMISSION-LINE PROPERTIES OF ONC STARS

ID	J	H	K	L	M	N	Q	Reference	$\Delta(I_C-K)$	$W_{\mathrm{Ca\ II}}$
3132.....	13.46	12.78	12.43	−9.99	−9.99	−9.99	−9.99	1, 4	−9.99	−1000.0
3157.....	13.75	13.26	12.78	−9.99	−9.99	−9.99	−9.99	1, 4	0.04	1.6
3126.....	12.05	11.34	11.16	−9.99	−9.99	−9.99	−9.99	1, 4	0.20	1.6
3153.....	−9.99	−9.99	12.41	−9.99	−9.99	−9.99	−9.99	4	1.59	0.0
3156.....	−9.99	−9.99	11.45	−9.99	−9.99	−9.99	−9.99	4	−9.99	−1000.0

NOTES.—Cols. (2)–(8) measured in magnitude; col. (9) measured in Å. Table 1 is presented in its entirety in the electronic edition of the Astronomical Journal. A portion is shown here for guidance regarding its form and content.

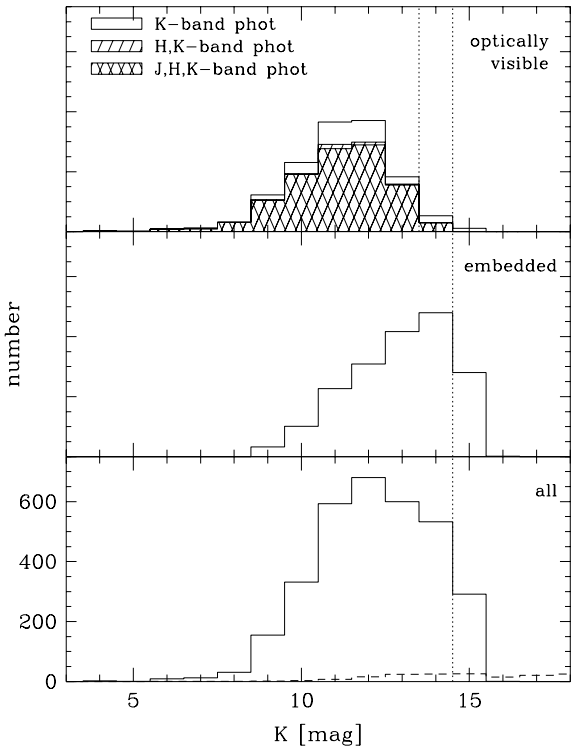

FIG. 1.—*K*-band magnitude functions for (*top panel*) optically visible ($I_C \lesssim 17.5$ mag) stars, (*middle panel*) optically invisible stars, and (*bottom panel*) the summed 2 μm population. Survey completeness to a limit of $K = 14.5$ mag is indicated, with the completeness extending only to $K = 13.5$ mag (indicated in the upper panel) for the derivation of $H-K$ and $J-H$ colors. The *H*-band and *J*-band completeness limits extend to $H \approx 14.5$ mag and $J \approx 15.5$ mag. Note that completeness is a strong function of projected cluster radius because of nebular contamination and source crowding in the inner cluster. The dashed line in the lower panel is the foreground star contamination based on the model of Jarrett (1992).

excesses more accurately than can be done from observed color-color diagrams alone (see the Appendix). We then explore trends in the near-infrared excess properties—interpreted as the manifestation of trends in circumstellar disk properties—with stellar age, stellar mass, and projected cluster radius.

2.4. *Completeness and Sensitivity*

How completely does the new infrared photometry combined with that in the literature sample the stellar population of the ONC? Answering this question requires investigation of the completeness of available data as a function of both limiting apparent magnitude and projected cluster radius.

Because of the strong gradients in point source crowding and in nebular brightness with cluster location, all infrared (and optical) surveys of the ONC region suffer from nonuniform depth in apparent magnitude with cluster radius. As was true for the assembly of our optical database, a "complete" survey in the infrared of the ONC stellar population can be achieved only by combining several different types of data sets. At present the stellar population of the ONC is sampled in the infrared (and in the optical) to the faintest magnitudes and at the highest spatial resolution in its central regions, fortunately just where such high-quality data is needed most in order to overcome the crowding and the nebulosity. The McCaughrean & Stauffer (1994) survey (0.18–0.32 arcsec pixel^{-1}) over the inner few arcminutes is reportedly complete to $K \sim 16$ mag. Over the remainder of the $\sim 25'$ survey radius considered here, the available imaging data is less deep and of lower resolution. The quoted limits of the Ali & Depoy (1995) survey (1.5 arcsec pixel^{-1}) are $K \sim 14.5$ mag averaged over the inner region of bright nebulosity and the outer parts of the nebula. Our own infrared survey includes data of slightly different resolution in the outer and inner cluster (0.8–1.3 arcsec pixel^{-1} for the imaging data and 15 arcsec aperture^{-1} for the photometer data on bright stars) and extends to $K = 13.5$–14.0 mag, $H = 14.5$–15.0 mag, and $J = 15.5$–16.0 mag, on average. Although "completeness" may not be defined by all of the above authors in the same manner, we can make some attempt to address the issue of completeness of the assembled infrared database empirically.

In terms of stellar parameters, the apparent brightness limits quoted above imply that at the distance of the ONC, we are sensitive to detection at *J*, *H*, *and K* of 1 Myr old stellar photospheres down to 0.1 $M_\odot$ as long as they are extincted by $A_V < 6$ mag. This age is slightly older than the mean thought to characterize the cluster ($\bar{\tau} = 0.8$ Myr), and this extinction is somewhat larger than the mean thought to characterize the optically visible stars ($A_V < 2$). For stars younger than 1 Myr, the surveys extend deeper in mass and in extinction than the limits quoted above. For stars with extinction values $A_V \leq 6$ mag, the surveys extend deeper in age and in mass than the limits quoted above. For stars more massive than 0.1 $M_\odot$, the surveys extend deeper in extinction and in age than the limits quoted above. In addition, the likely presence of near-infrared excess owing to circumstellar dust renders these physical completeness limits the most pessimistic of possible values.

The completeness of the infrared database for optically identified stars also can be investigated as a function of projected radius, as is shown in Figure 5. At radii $\gtrsim 0.5$ pc the infrared photometry is fairly uniformly complete with radius: $\sim 95\%$ of optically visible stars have *K*-band photometry with $\sim 80\%$ having full *JHK* data. Stars with *K*-band measurements but lacking *J*- and *H*-band photometry typically lie near or just below the infrared survey completeness limits based on the I_C-K, I_C-H, and I_C-J colors expected from stellar photospheres. Inside of 0.5 pc, good near-infrared photometry is still unavailable for a significant fraction of the optically visible stars, especially at the *J* and *H* bands. The dominant reason for this is crowding on the typically lower resolution near-infrared images (compared with the optical [*HST*] images from which the sources were initially identified).

Finally, there do not appear to be any biases in the distribution of stars with and without near-infrared photometry in the $V-(V-I_C)$ color-magnitude diagram. Completeness of the optical database is discussed in Hillenbrand (1997). In summary, existing near-infrared surveys penetrate to sufficient depth to sample the optically visible ONC stellar population over its full range in mass and age and so to enable the detection of circumstellar disks surrounding stars of all masses and ages.

3. DETECTION OF CIRCUMSTELLAR DISKS FROM NEAR-INFRARED EXCESS

In this section we describe our methodology for computing near-infrared excesses. We have combined the infrared photometry (*J*, *H*, *K*) presented in this paper with the optical photometry (V, I_C) and spectral type information

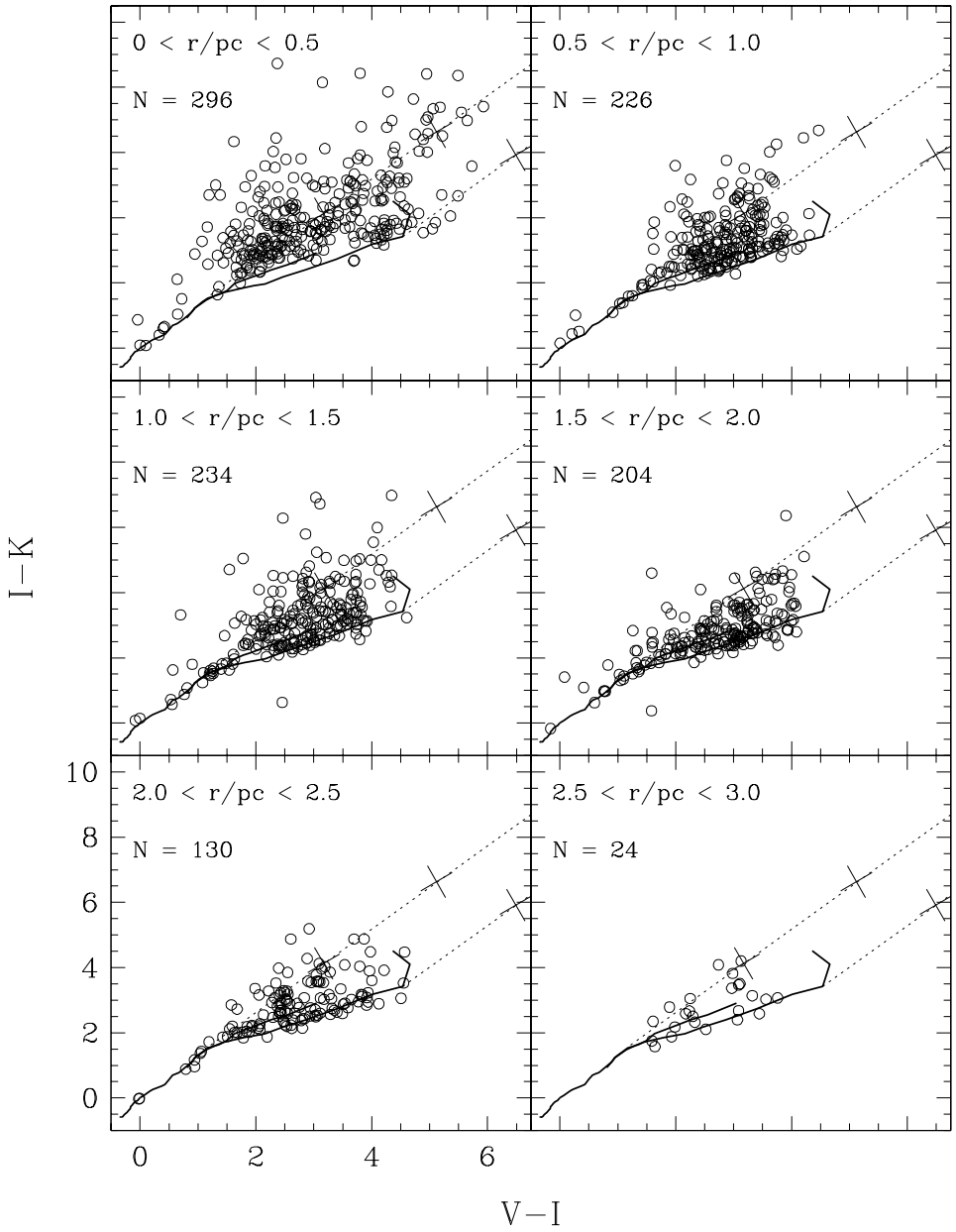

FIG. 2.—$(V-I_C)$-(I_C-K) color-color diagram as a function of projected cluster radius. Heavy solid lines indicate the loci of colors expected for main-sequence dwarfs (down to M9) and post–main-sequence giants (down to M5), while dotted lines drawn from the extrema of the sequences are reddening vectors. Crosses mark intervals of 5 mag of visual extinction along the reddening vectors. The total number of stars with V-, I-, and K-band photometry is 1114.

(derived from ≈5000–9000 Å spectra) presented in Hillenbrand (1997). The subsample of optical stars with spectral types is thought to be unbiased with respect to stellar mass and stellar age and fully representative of the ONC population over the extinction range $A_V < 2.5$ mag; 813 of these 934 stars have infrared photometry. We first define a photometric index with which to search for near-infrared excesses above photospheric values and investigate the impact of observational errors on our ability to detect near-infrared excesses for stars of different apparent brightness and spectral type. Next, we discuss theoretical models in which the near-infrared excess is interpreted as arising from heating processes (irradiation and accretion) associated with circumstellar disks, and we compare the magnitude of the expected near-infrared excesses with the accuracy achievable from our data. In the next section we present our results.

3.1. *Observational Diagnostic*

We study the near-infrared excess using an index based on I_C-K colors. For our particular photometric data set (VI_C, JHK), the I_C-band fluxes are least affected by circumstellar activity and so are typically dominated by photospheric emission, while emission arising from accretion disks is maximized at K-band. The main disadvantage of this diagnostic is that the optical and the infrared data were not obtained contemporaneously, so we are susceptible to

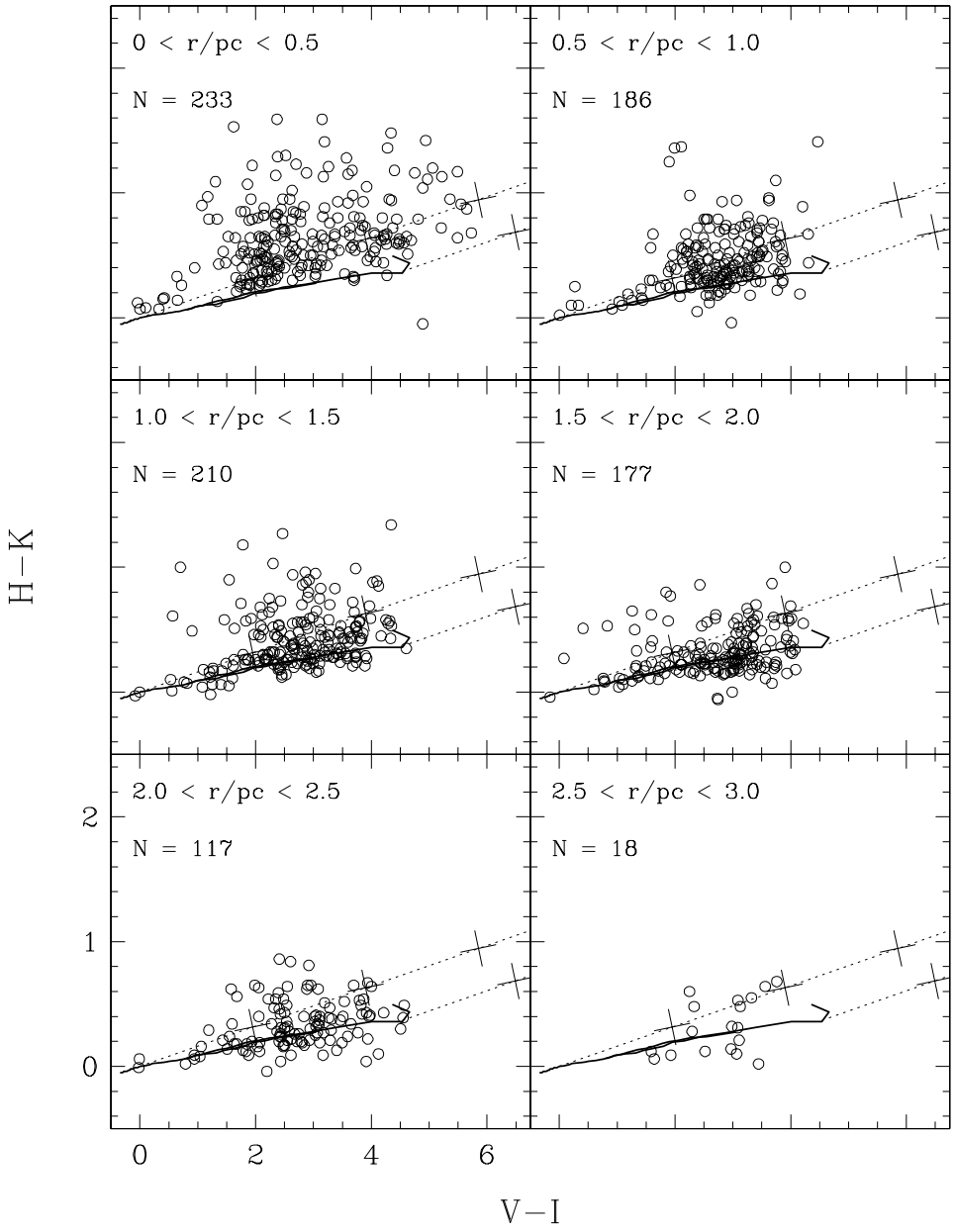

FIG. 3.—$(V-I_C)$-$(H-K)$ color-color diagram as a function of projected cluster radius. Heavy solid lines indicate the loci of colors expected for main sequence dwarfs (down to M9) and post–main-sequence giants (down to M5; note that the dwarf and giant sequences are degenerate in $H-K$), while dotted lines drawn from the extrema of the sequences are reddening vectors. Crosses mark intervals of 5 mag of visual extinction along the reddening vectors. The total number of stars with V-, I-, H-, and K-band photometry is 941.

the effects of photometric variability.[2]

To calculate the near-infrared excess we make several assumptions: (1) the observed $V-I_C$ colors are photospheric in origin and suffer only the effects of reddening (but not circumstellar excess); (2) the observed I_C-K colors measure the photospheric color plus the amount of circumstellar excess at 2 μm, and are also reddened; (3) the spectral types provide us with knowledge of the underlying stellar colors, $(V-I_C)_{\rm photosphere}$ and $(I_C-K)_{\rm photosphere}$, and so allow us to account accurately for the effects of reddening; and (4) the photospheric colors are similar to those of dwarf standard stars, neglecting the possibility that 1 Myr old stars may have colors intermediate between dwarfs and giants and any possible color anomalies arising from surface magnetic activity. We then define a quantity used to measure the magnitude of the near-infrared excess, $\Delta(I_C-K)$,

$$\Delta(I_C-K) = (I_C-K)_{\rm observed} - 0.5A_V - (I_C-K)_{\rm photosphere},$$

where the first term is the observed I_C-K color, the second term is the contribution of reddening calculated from the extinction values derived from the $V-I_C$ colors

[2] One might mitigate some of the errors introduced by photometric variability by making use of an alternate index, such as $\Delta(H-K)$. We choose $\Delta(I_C-K)$ instead of $\Delta(H-K)$ because (1) the magnitude of expected excess from a passive disk is larger in $\Delta(I_C-K)$ than in $H-K$, (2) the magnitude of the gradient in photospheric colors is also larger in $\Delta(I_C-K)$ than in $H-K$, and (3) the sample of stars with both $\Delta(I_C-K)$ and K magnitudes is larger than the sample of stars with H and K magnitudes.

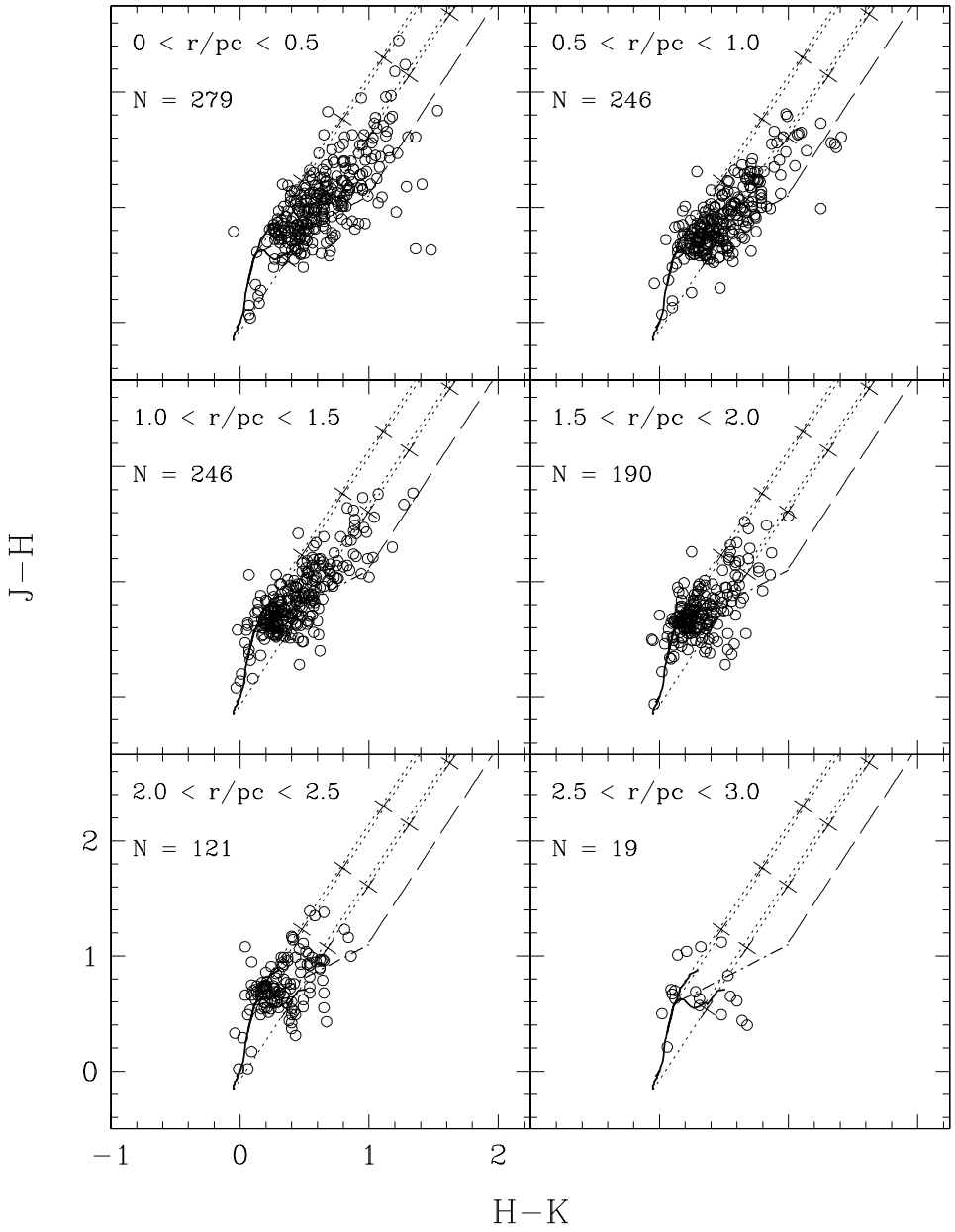

FIG. 4.—$(J-H)$-$(H-K)$ color-color diagram as a function of projected cluster radius. Heavy solid lines indicate the loci of colors expected for main sequence dwarfs (down to M9) and post–main-sequence giants (down to M7), while dotted lines drawn from the extrema of the dwarf and giant sequences are reddening vectors. Crosses mark intervals of 5 mag of visual extinction along the reddening vectors. The dot-dashed line represents the locus of colors occupied by dereddened classical T Tauri stars in Taurus-Auriga (see Meyer et al. 1997) and is also accompanied by a reddening vector. The total number of optically visible stars with J-, H-, and K-band photometry is 1101.

as in Hillenbrand (1997), and the third term is the contribution of the underlying stellar photosphere. If, as we demonstrate in § 7, a large fraction of the stars in our sample have accretion disks, then the observed V-band and I_C-band fluxes *may* not be completely reddened photospheric; they may show the effects of both "red excess" from the relatively cool disk (more so at I_C band) and "blue excess" from the hot accretion zone near to the star (more so at V band). The spectroscopic veiling measurements of Basri & Bathala (1990) and of Hartigan et al. (1991) show that *for those stars with accretion disks*, the ratio of "blue excess" to photospheric flux systematically decreases with wavelength from $\sim$0.8 at 5500 Å to $\sim$0.3 at 8500 Å. In the absence of similar quality data that would allow us to evaluate directly the amount of contamination from the "blue excess" at the V band and I_C band, we proceed under the assumptions outlined above.

How accurately can we calculate $\Delta(I_C-K)$ from the ONC data? Since our definition of $\Delta(I_C-K)$ depends on the observed colors and on the colors assumed for the underlying star, both random and systematic errors are present. Contributions to the random error come from photometric error, which increases toward fainter magnitudes, and from time variability of the photometry. Contributions to the systematic error derive from errors in the spectral typing. Although spectral typing errors are in principle random errors, in the calculation of $\Delta(I_C-K)$ they act in practice like systematic errors, since they affect both the colors assumed for the underlying star and the extinction estimate, resulting in most cases to reduce the value of

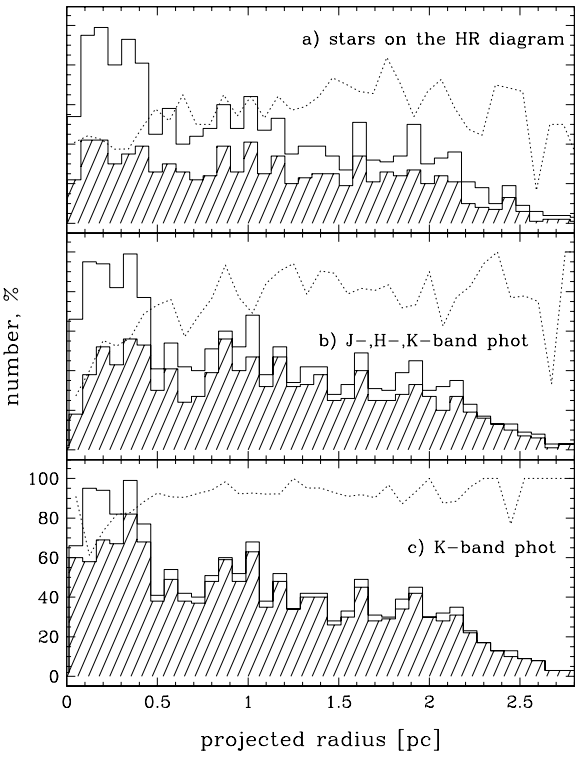

FIG. 5.—Completeness with projected radius, relative to the I_C-band sample. The open histogram indicates the radial distribution of stellar sources identified at I_C band, and is the same on all three panels. The hatched histogram indicates the radial distribution of sources (*top panel*) located on the H-R diagram, (*middle panel*) for which we have all of *J*-, *H*-, and *K*-band photometry, and (*bottom panel*) for which we have *K*-band photometry. The "center" of the cluster is arbitrarily defined as the position of θ^1C Ori. The dotted line in each panel indicates the fractional completeness relative to the I_C-band data. Note the drop in fractional completeness toward the inner cluster for stars with $J-H$ and $H-K$ colors.

$\Delta(I_C-K)$, except when the extinction is large. If a star is misclassified too early in type, the intrinsic stellar colors ($V-I_C$ and I_C-K) will be underestimated and the value of A_V will be overestimated. Conversely, if a star is misclassified too late in type, the intrinsic stellar colors will be overestimated and the value of A_V underestimated. The summed consequence on errors in our $\Delta(I_C-K)$ diagnostic is a complex function of the true spectral type, the true amount of extinction suffered by the system, and the magnitude of the spectral typing error, as we now describe.

We estimated the errors in the values of $\Delta(I_C-K)$ calculated from our data as a function of both spectral type (SpT = O5–M6) and extinction (A_V = 0–2 mag). We assume spectral typing errors of $\frac{1}{2}$ spectral subclass and 1 spectral subclass (we estimate the accuracy of our spectral types to be $\pm\frac{1}{2}$ subclass for stars later than K7, ±1 subclass for stars K0–K7, ±3–4 subclasses for stars F0–G8 where red spectral classification is most difficult, and ±1 subclass for stars earlier than F0; see Hillenbrand 1997 for further discussion). We assume photometric errors with magnitude as measured from our optical/infrared photometry. In the $A_V = 0$ mag case, the errors induced in $\Delta(I_C-K)$ by spectral misclassification are negative [i.e., $\Delta(I_C-K)$ is reduced from its true value] for all spectral types; the only exception to this is when the latest type stars ($\geq$M6) are misclassified too late in type. In other words, it is unlikely for $\Delta(I_C-K)$ to be estimated at larger than its true value. In the A_V = 1–2 cases, however, positive errors in $\Delta(I_C-K)$ are possible, but again *only* in the improbable scenario of misclassifying a late-type star ($\geq$K5) too late in type. We tabulate the results of these simulations in Table 2. The median spectral type for our optically visible ONC sample is M3 and the median extinction is $A_V = 0.9$ mag. Generalizing our results, uncertainties in the $\Delta(I_C-K)$ diagnostic are negligible for earlier spectral types (less than 0.05 mag for stars $\lesssim$K2), 0.1–0.3 mag for spectral types K2–M3, and largest for the latest spectral types where misclassification causes relatively larger errors in the intrinsic stellar colors. It is more likely (because of the possible presence of excess emission from optical continuum veiling or to poor nebular subtraction during the data reduction) for a star to be called earlier than it really is rather than later, and thus the expectation is that the errors in $\Delta(I_C-K)$ are primarily negative [i.e., $\Delta(I_C-K)$ is reduced from its true value]. We note that this introduces the possibility of measuring absolutely negative [$\Delta(I_C-K) < 0$] values for $\Delta(I_C-K)$ if the intrinsic $\Delta(I_C-K)$ is positive but small or zero. We also note that these error estimates do not take photometric variability, which for these stars can be several tenths of a magnitude at I_C band (Choi & Herbst 1996) *and* at *K* band (M. F. Skrutskie, unpublished data) into account.

The next question to be addressed is whether the accuracy in our determination of the magnitude of the near-infrared excess from $\Delta(I_C-K)$ exceeds that needed to detect circumstellar disks surrounding stars of all masses and ages represented in the ONC. What magnitude of near-infrared excess emission would we expect from disks surrounding stars spanning the range of masses and ages characterizing our sample?

3.2. *Theoretical Expectations*

Complete appreciation of our ability to detect circumstellar material requires an understanding of the magnitude of the effect we are trying to detect, i.e., knowledge of the expected excesses over stellar photospheric flux levels. We adopt a model in which the near-infrared excess is attributed to heating processes (irradiation and accretion) associated with circumstellar disks. Similar accretion disk physics can produce vastly different observational signatures for stars of different temperature (i.e., mass) and radius (i.e., age). The wide range in stellar mass and age included in our sample makes understanding the inherent systematics with mass and age especially crucial. How accurate must our chosen diagnostic for circumstellar disks, $\Delta(I_C-K)$, be in order to detect circumstellar material around stars of different mass and age, given the plausible ranges in disk parameters?

In order to estimate the amount of near-infrared excess expected from disks of various accretion rate, inner disk hole size, and inclination surrounding stars of different temperature and radius (i.e., mass and age), Calvet's models of stellar + disk atmospheres were used. The models include both irradiative heating of the disk by the star from above and accretional heating of the disk from within and are more fully described in Calvet et al. (1991, 1992; see also Meyer, Calvet, & Hillenbrand 1997). The central stars were chosen to have temperatures corresponding to spectral types K7, M1, M3, M5, M7, and M9 and thus masses according to the pre–main-sequence evolutionary tracks of D'Antona & Mazzitelli (1994) in the range 0.40–0.05 $M_\odot$.

TABLE 2

ERRORS IN CALCULATION OF $\Delta(I_C-K)$ FOR 1 MYR OLD STARS AT 470 pc

SPECTRAL TYPE	$V-I_C$	I_C-K	σV	σI_C	σK	$A_V=0$				$A_V=1$				$A_V=2$			
						1 late	1 early	½ late	½ early	1 late	1 early	½ late	½ early	1 late	1 early	½ late	½ early
O9	−0.34	−0.58	0.00	0.00	0.00	−0.01	−0.04	−0.01	−0.02	0.04	−0.04	0.02	−0.02	0.04	−0.04	0.02	−0.02
B0.....	−0.30	−0.57	0.00	0.00	0.00	−0.08	−0.04	−0.04	−0.02	−0.03	−0.04	−0.01	−0.02	−0.03	−0.04	−0.01	−0.02
B1.....	−0.26	−0.49	0.00	0.00	0.00	−0.04	0.03	−0.02	0.01	−0.00	0.03	−0.00	0.01	−0.00	0.03	−0.00	0.01
B2.....	−0.23	−0.45	0.00	0.00	0.00	−0.08	0.00	−0.04	0.00	−0.03	0.00	−0.01	0.00	−0.03	0.00	−0.01	0.00
B3.....	−0.19	−0.37	0.00	0.00	0.00	−0.10	0.03	−0.05	0.01	−0.06	0.03	−0.03	0.01	−0.06	0.03	−0.03	0.01
B5.....	−0.16	−0.27	0.00	0.00	0.00	−0.04	0.06	−0.02	0.03	−0.01	0.06	−0.01	0.03	−0.01	0.06	−0.01	0.03
B6.....	−0.14	−0.23	0.00	0.00	0.00	−0.05	0.01	−0.03	0.01	−0.02	0.01	−0.01	0.01	−0.02	0.01	−0.01	0.01
B7.....	−0.12	−0.18	0.00	0.00	0.00	−0.06	0.02	−0.03	0.01	−0.02	0.02	−0.01	0.01	−0.02	0.02	−0.01	0.01
B8.....	−0.09	−0.12	0.00	0.00	0.00	−0.05	0.02	−0.03	0.01	0.01	0.02	0.01	0.01	0.01	0.02	0.01	0.01
B9.....	−0.04	−0.07	0.00	0.00	0.00	−0.07	−0.01	−0.04	−0.01	−0.02	−0.01	−0.01	−0.01	−0.02	−0.01	−0.01	−0.01
A0	0.00	0.00	0.00	0.00	0.00	−0.08	0.02	−0.04	0.01	0.01	0.02	0.00	0.01	0.01	0.02	0.00	0.01
A2	0.07	0.08	0.00	0.00	0.00	−0.13	−0.01	−0.07	−0.00	−0.00	−0.01	−0.00	−0.00	−0.00	−0.01	−0.00	−0.00
A5	0.17	0.21	0.00	0.00	0.00	−0.05	0.00	−0.03	0.00	0.01	0.00	0.01	0.00	0.01	0.00	0.01	0.00
A7	0.22	0.26	0.00	0.00	0.00	−0.11	−0.01	−0.06	−0.01	0.08	−0.01	0.04	−0.01	0.08	−0.01	0.04	−0.01
F0.....	0.37	0.37	0.00	0.00	0.00	−0.05	−0.08	−0.03	−0.04	0.03	−0.08	0.01	−0.04	0.03	−0.08	0.01	−0.04
F2.....	0.43	0.42	0.00	0.00	0.00	−0.15	−0.03	−0.08	−0.01	−0.06	−0.03	−0.03	−0.01	−0.06	−0.03	−0.03	−0.01
F5.....	0.50	0.57	0.00	0.00	0.00	−0.15	0.06	−0.08	0.03	−0.03	0.06	−0.02	0.03	−0.03	0.06	−0.02	0.03
F8.....	0.59	0.72	0.00	0.00	0.00	−0.03	0.03	−0.02	0.02	0.02	0.03	0.01	0.02	0.03	0.02	0.02	0.01
G0	0.63	0.75	0.00	0.00	0.00	−0.03	−0.02	−0.02	−0.01	0.02	−0.02	0.01	−0.01	0.03	−0.03	0.02	−0.02
G2	0.67	0.78	0.00	0.00	0.00	−0.30	−0.02	−0.15	−0.01	−0.03	−0.02	−0.02	−0.01	−0.02	−0.03	−0.01	−0.02
K0	0.88	1.08	0.00	0.00	0.00	−0.16	0.03	−0.08	0.02	−0.06	0.02	−0.03	0.01	−0.06	0.02	−0.03	0.01
K2	0.95	1.24	0.00	0.00	0.00	−0.39	0.07	−0.20	0.04	0.09	0.06	0.05	0.03	0.09	0.06	0.05	0.03
K5	1.32	1.63	0.00	0.00	0.01	−0.07	−0.09	−0.03	−0.05	0.14	−0.13	0.09	−0.09	0.14	−0.13	0.09	−0.09
K7	1.45	1.71	0.00	0.00	0.01	−0.13	−0.10	−0.06	−0.05	0.36	−0.14	0.20	−0.09	0.36	−0.14	0.20	−0.09
M0.....	1.80	1.85	0.00	0.01	0.05	0.01	−0.38	0.04	−0.23	0.20	−0.36	0.12	−0.20	0.19	−0.36	0.12	−0.20
M1.....	1.96	1.91	0.01	0.01	0.05	0.03	−0.23	0.06	−0.16	0.28	−0.23	0.18	−0.16	0.28	−0.23	0.18	−0.16
M2.....	2.16	1.97	0.01	0.01	0.05	−0.12	−0.28	−0.02	−0.18	0.27	−0.28	0.18	−0.18	0.27	−0.28	0.18	−0.18
M3.....	2.47	2.18	0.02	0.01	0.05	−0.12	−0.29	−0.01	−0.19	0.38	−0.29	0.24	−0.19	0.46	−0.37	0.32	−0.28
M4.....	2.86	2.40	0.03	0.02	0.05	−0.20	−0.41	−0.03	−0.27	0.37	−0.48	0.37	−0.34	0.70	−0.63	0.53	−0.50
M5.....	3.39	2.73	0.05	0.03	0.10	−0.16	−0.58	0.04	−0.41	0.46	−0.70	0.56	−0.53	0.76	−0.70	0.56	−0.53
M6.....	4.01	3.12	0.05	0.04	0.20	−0.03	−0.76	0.16	−0.56	0.46	−0.76	0.56	−0.56	0.76	−0.76	0.56	−0.56

NOTES.—Cols. (2)–(18) are measured in magnitude. Cols. (1)–(3): spectral type, $(V-I_C)$ color, and (I_C-K) color of the dwarf photosphere; Cols. (4)–(6): photometric error at V, I_C, and K; Cols. (7)–(10): total error in $\Delta(I_C-K)$ caused by misclassifying the star too late and too early in type by 1 subclass and by ½ subclass in the case of no extinction; Cols. (11)–(14): same as Cols. (7)–(10) for the case of $A_V = 1$ mag; and Cols. (15)–(18): same as Cols. (7)–(10) for the case of $A_V = 2$ mag. The mean spectral for our ONC sample is M3 and the mean extinction is less than 1 mag. Spectral typing errors are more likely to be in the sense of classifying a star too early rather than too late; see text.

The stars have radii in the range 1.25–3.25 $R_\odot$, corresponding to ages in the range 0.1–10 Myr depending on the mass. For each combination of M_* and R_*, a grid of disk models sampling (1) accretion rates of 10^{-9} (irradiation-dominated), 10^{-8}, 10^{-7}, and 10^{-6} (accretion-dominated) $M_\odot$ yr^{-1}, (2) inner disk hole sizes of 1 (no hole), 3, and 6 R_*, and (3) inclination values of 0°, 30°, 60°, and 80° was created. The total spectral energy distribution is calculated in the models by considering both irradiation of the disk from above by the stellar radiation field and heating of the disk from within by viscous accretion processes. We show an example spectral energy distribution in order to illustrate the effects of accretion, inner disk holes, and inclination in Figure 6; the central star has spectral type M3 (mass $\sim$0.23 $M_\odot$ for an age of 1 Myr), near the median mass of 0.25 $M_\odot$ for the ONC, and radius 2.0 $R_\odot$ (age $\sim$0.2 Myr at 0.25 $M_\odot$), near the mean radius for the low-mass ONC population of 1.8 $R_\odot$.

In the previous subsection, we introduced the quantity $\Delta(I_C-K)$ as a measure of the magnitude of the infrared excess. As was emphasized above, this diagnostic has the advantage that in young stellar objects, I_C-band magnitudes are typically least contaminated by circumstellar emission while progressively shorter and longer wavelengths are increasingly contaminated by "blue excess" and "red excess," respectively. For our VI_C, JHK photometric database, the $\Delta(I_C-K)$ index thus provides the longest lever arm on the infrared excess.

From the Calvet et al. models, the near-infrared excess is generally larger (1) for more rapidly accreting disks, (2) for disks with smaller inner holes, and (3) for less inclined disks. However, the stellar parameters ($M/M_\odot$ and $R/R_\odot$) are also extremely important.

In Figure 7 we show the expected variation of $\Delta(I_C-K)$ with dereddened $V-I_C$ color (a surrogate for stellar temperature/mass) for three different values of the stellar radius: $R_* = 3.25, 2, 1.25\ R_\odot$. In our initial discussion of the magnitude of the near-infrared excess expected from accretion

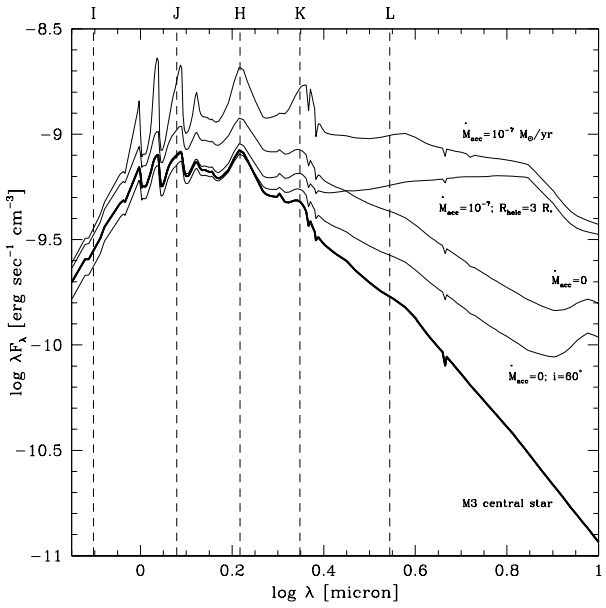

FIG. 6.—Spectral energy distribution for a star/disk system. The heavy solid line represents the spectral energy distribution of an unreddened M3 star (near the mean spectral type in the ONC), while the light solid lines indicate the total spectral energy distributions expected from the irradiation + accretion models of Calvet et al. for the M3 star when surrounded by circumstellar disks of various accretion, inner disk hole, and inclination properties. Compared with the nonaccreting no-hole pole-on disk, inclined disks reduce the magnitude of the infrared excess at all wavelengths, while inner disk holes reduce the infrared excess at short near-infrared wavelengths only, and accreting disks increase the magnitude of the infrared excess modulo the strong absorption bands that appear at higher accretion rates. The central wavelengths of the I, J, H, K, and L bandpasses are indicated with vertical dashed lines.

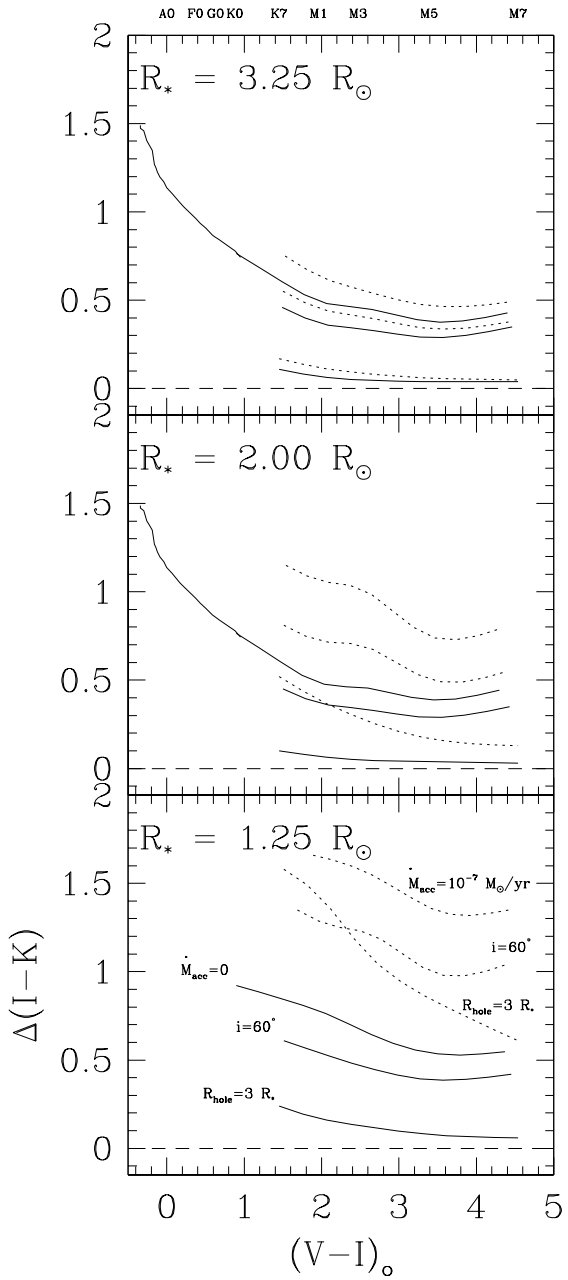

FIG. 7.—Predicted I_C-K excesses for star + disk systems. The three panels show from top to bottom, different values for the stellar radius, 3.25, 2.00, and 1.25 $R_\odot$. In each panel, solid lines represent irradiation-dominated disks while dotted lines are for $\dot{M}_{acc} = 10^{-7}\ M_\odot$ yr^{-1} disks. For each accretion rate we show the excesses expected from a pole-on disk (*top line*), a disk inclined at 60° (*middle line*), and a pole-on disk with an inner hole of 3 R_* (*bottom line*). The translation from photospheric $V-I_C$ color to spectral is given at the top. The expected magnitude of the near-infrared excess increases toward (1) higher stellar mass, (2) smaller stellar radii, (3) higher accretion rates, (4) smaller inner disk hole sizes, and (5) smaller values of system inclination.

disks, we hold the stellar radius constant at $R_* = 2\ R_\odot$ (*middle panel*) and examine trends with stellar mass; we consider the trends with stellar radius at fixed mass below. Both irradiation-dominated (*solid lines*) and accretion-dominated (*dotted lines*) disks are shown in Figure 7, and in both cases the magnitude of the quantity $\Delta(I_C-K)$ decreases steadily toward redder intrinsic $V-I_C$ colors (i.e., cooler temperatures and lower mass stars). For disks in which irradiation is the main source of heating, the disks become less luminous toward later spectral types as the stellar luminosity decreases at constant radius, leading to smaller values of the $\Delta(I_C-K)$ excess. For accreting disks, the disks also become less luminous toward later spectral types as the depth of the potential well decreases at constant $\dot{M}_{\rm acc}$, leading to smaller values of the $\Delta(I_C-K)$ excess. The magnitude of the quantity $\Delta(I_C-K)$ also decreases toward bigger (i.e., younger) stars. This is due both to a decrease in the potential well depth for bigger stars and to a decrease in contrast between the disk and the star as the stellar bolometric luminosity goes up. For a fixed accretion rate, increasing the stellar radius at constant stellar mass decreases the magnitude of the near-infrared excess, while decreasing the stellar radius increases the magnitude of the near-infrared excess. Thus it is around the youngest objects (those with the largest stellar radii) that disk detection appears to be the most difficult. However, if as predicted by disk evolutionary theories, accretion rates are higher at earlier evolutionary phases, for very young stars the combination of intrinsic disk physics and contrast effects may in fact counteract each other to produce detectable disks.

We also show in Figure 7 the effects of inclination and inner disk holes, both of which reduce the magnitude of $\Delta(I_C-K)$ from the pole-on, $R_{\rm inner} = 1\ R_*$ case. Inclination angles are expected to be randomly distributed from 0° to 90°. Inner disk holes, i.e., the truncation of circumstellar disks surrounding young stars at a radius roughly corresponding to the balance point between pressure inward from viscous (accretion) energy and pressure outward from the stellar magnetic field, are suggested from theoretical work in the literature (Shu et al. 1994). Although no firm numbers for the sizes of inner disk holes have been established, estimates in the 2–6 R_* (4–12 $R_\odot$ for our canonical 2 $R_\odot$, $\lesssim$1 Myr low-mass star) are consistent with available observational material (Meyer et al. 1997; Hartmann, Hewett, & Calvet 1994; Edwards et al. 1994; Muzerolle, Calvet, & Hartmann 1998). In the irradiation-dominated ($\dot{M}_{\rm acc} = 10^{-9}\ M_\odot\ {\rm yr}^{-1}$) case, an inner disk hole size of 3 R_* is sufficient to remove nearly all near-infrared excess for stars later than M1 ($M \lesssim 0.31\ M_\odot$)! Quantitative estimates of inner disk hole sizes await the attainment of flux-calibrated spectra throughout the near-infrared.

In summary, the amount of near-infrared excess expected from circumstellar disks is a function of both the mass and the radius of the central star, as well as of the disk properties. The magnitude of the near-infrared excess is expected to increase with increasing stellar mass and with decreasing stellar radius. The magnitude of the near-infrared excess is also expected to increase with increasing accretion rate, with decreasing inner disk hole size, and with decreasing inclination angle, although specific combinations of these three parameters can produce results that deviate from the general trends (see Meyer et al. 1997; Calvet et al. 1999). Thus, given the multiplicity of influences on the magnitude of the near excess from disk properties, great care is needed in diagnosing the presence of disks using near-infrared excesses. We conclude[3] that from the $\Delta(I_C-K)$ index, disks with accretion rates $\dot{M}_{\rm acc} > 10^{-9}\ M_\odot\ {\rm yr}^{-1}$ should be detectable around low-mass ($M > 0.08\ M_\odot$) young stellar objects at all inclinations unless the disks have inner holes. We may still detect disks with inner holes $\lesssim 3\ R_*$ around low-mass stars—if the accretion rates are high enough, $\dot{M}_{\rm acc} > 10^{-7.5}\ M_\odot\ {\rm yr}^{-1}$. Disk detection around higher mass stars ($M \gtrsim 3\ M_\odot$) is relatively straightforward given the large contrast between the relatively hotter star and the much cooler pure-irradiation or even low-$\dot{M}_{\rm acc}$ disk.

4. OBSERVED INFRARED CONTINUUM EXCESSES IN OPTICALLY VISIBLE STARS

In this section we present the observational results for our circumstellar disk diagnostic $\Delta(I_C-K)$ (§ 3.1) in comparison with the theoretical expectations (§ 3.2). We also illustrate some of the patterns with stellar (and cluster) parameters manifest in the measured magnitude of the near-infrared excess.

We show the quantity $\Delta(I_C-K)$, calculated as described in § 3.1 for the 813 ONC stars with optical/infrared photometry and spectral types, plotted against dereddened $V-I_C$ color, in Figure 8. This display is analogous to Figure 2 in that stellar mass and cluster radius are represented here as they are in the pure observational plane; however, the data points have been corrected along both axes for the color effects of extinction and along the ordinate for the stellar photosphere. The expected changes in $\Delta(I_C-K)$ introduced by making a ± 1 subclass error in the spectral type for a star having an extinction of $A_V = 0$ mag and $A_V = 1$ mag are indicated: see Table 2. As discussed above, these changes are larger for stars of later spectral type owing to the rapid variation of color with spectral type, and they usually act in the negative direction, except when a star with $A_V \gtrsim 0.5$ mag is classified too late in type (an unlikely error). Note also that we believe the spectral typing errors to be closer to $\frac{1}{2}$ spectral subclass than 1 subclass for M stars. The peak of the spectral type distribution around M3 means that for most stars in the sample the uncertainties are expected to be well less than 0.15 mag in $(V-I_C)_0$ and 0.3 mag in $\Delta(I_C-K)$.

[3] How does the magnitude of the excess at K band, H band, and J band generally behave as a function of the stellar and disk parameters? At constant stellar radius ($R_* = 2\ R_\odot$), in the case of pole-on ($i = 0°$) irradiation-dominated ($\dot{M}_{\rm acc} \leq 10^{-9}\ M_\odot\ {\rm yr}^{-1}$) disks, monochromatic excess above the stellar photosphere is larger than 0.2 mag at K band and H band for all spectral types. At J band, however, the excess disappears beyond a spectral type of M7 ($M \lesssim 0.08\ M_\odot$) as the brightness of the stellar photosphere exceeds the brightness of the disk by more than an order of magnitude. For more rapidly accreting disks ($\dot{M}_{\rm acc} = 10^{-8}$, 10^{-7}, $10^{-6}\ M_\odot\ {\rm yr}^{-1}$), monochromatic excess is discernible at all of the K, H, and J bandpasses for all spectral types. An inner disk hole size of 3 R_* removes entirely the excesses at K, H, J for all stars later than M2 ($M \lesssim 0.27\ M_\odot$) for an accretion rate $\dot{M}_{\rm acc} \leq 10^{-8}\ M_\odot\ {\rm yr}^{-1}$ and for all stars later than M6 ($M \lesssim 0.11\ M_\odot$) for an accretion rate $\dot{M}_{\rm acc} \leq 10^{-7}\ M_\odot\ {\rm yr}^{-1}$. These numbers are for the case of a pole-on system. In the most likely case of $i = 60°$, disks without inner holes are still detectable around stars of all masses, but disks with inner holes of size 3 R_* are not detectable unless the accretion rates exceed a few $10^{-8}\ M_\odot\ {\rm yr}^{-1}$. Even in the case of $\dot{M}_{\rm acc} = 10^{-7}\ M_\odot\ {\rm yr}^{-1}$, disks inclined at 60° with 3 R_* holes are not detectable beyond a spectral type of M5 ($M \lesssim 0.14\ M_\odot$). In order to diagnose inclined disks with inner holes around such extremely low-mass stars, it appears necessary to sample spectral energy distributions at wavelengths *longer than* $\sim$3.5 μm (L band). As a reminder, the apparent peak of the mass function in the ONC occurs at spectral type M3 ($M \approx 0.25\ M_\odot$).

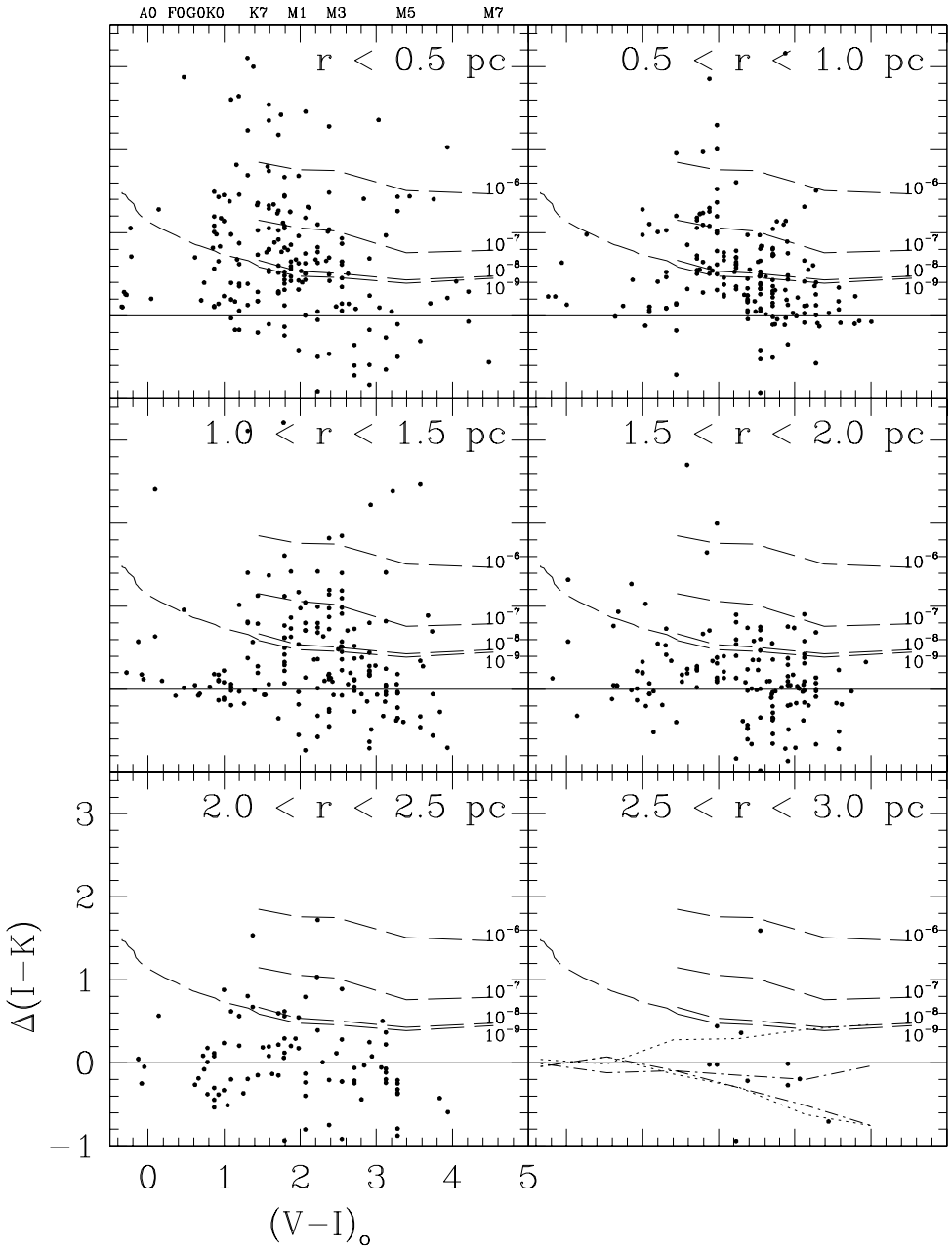

FIG. 8.—Near-infrared excess diagnosed from $\Delta(I_C-K)$ vs. dereddened optical color, as a function of projected cluster radius. The quantity $\Delta(I_C-K)$ is calculated for 813 stars by subtracting the contributions of reddening and the underlying stellar photosphere from the observed (I_C-K) color. Including stars of all spectral types, the mean value of $\Delta(I_C-K)$ is 0.36 mag. Dashed lines indicate the excesses expected from pole-on irradiation + accretion disks with no inner disk holes, with accretion rates as labeled. These calculations assume a stellar radius of 2 $R_\odot$ (near the ONC mean); see Fig. 7 for the effects of varying the stellar radius. In the lower right panel we indicate the formal errors in $\Delta(I_C-K)$ induced by making a one spectral subclass error for the cases of $A_V = 0$ (*inner two dot-dashed lines*) and $A_V = 1$ (*outer two dotted lines*). The upper line for each extinction value is the error caused by classifying a star too late in type (unlikely), while the lower line is the error caused by classifying a star too early in type.

For comparison, we also show as dashed lines the excesses expected from pole-on accretion disks surrounding $R_* = 2$ $R_\odot$ stars; the lowest line in these figures represents the excess expected from an irradiation-dominated disk, while higher lines indicate increasing values of the accretion rate, as labeled.

Values of the infrared excess not only above zero but also above the pure-irradiation disk line can be understood in terms of accretion disk systems. The $\dot{M}_{acc}$'s in these cases produce disk heating in excess of that produced by irradiation from the central star. Values of the infrared excess below the reprocessing disk line but above zero can be understood as inclined systems and/or disks with inner disk holes. The $\dot{M}_{acc}$'s in these cases are insufficient to overcome the combined effects of inclination and inner holes. Values of the infrared excess below zero can be understood in terms

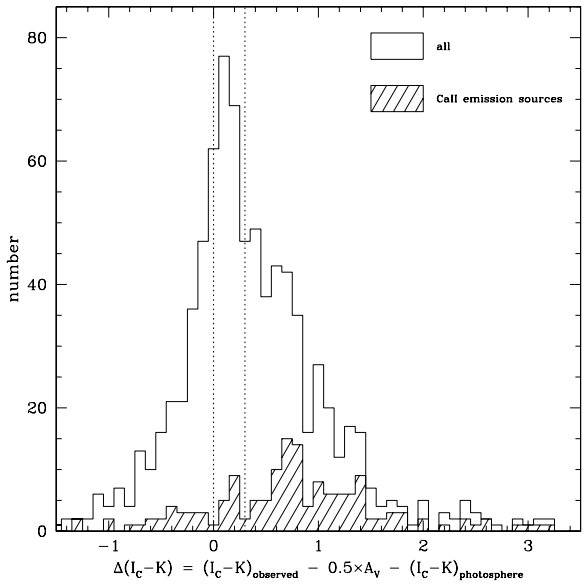

FIG. 9.—Histogram of near-infrared excesses. The distribution of $\Delta(I_C-K)$ is shown both for the full sample of stars with V-, I_C-, and K-band photometry and optical spectral types (*open histogram*) and for that subsample with the Ca II triplet ($\lambda\lambda$8498, 8542, and 8662) in emission (*hatched histogram*; see § 7.2). Negative values of $\Delta(I_C-K)$ are attributed to errors either in the photometry or with the spectral types (see text); note that some of the Ca II sources, commonly interpreted as objects undergoing accretion, have negative values of $\Delta(I_C-K)$ highlighting our inability to detect *all* accretion disk systems with our formalism. Vertical dotted lines indicate no infrared excess, $\Delta(I_C-K)=0$, and the average value for the sample, $\Delta(I_C-K)\approx 0.3$ mag.

of errors in deriving the $\Delta(I_C-K)$ diagnostic,[4] as is illustrated in the lower right panel.

Including all 813 ONC stars in Figure 8 (those located at all projected cluster radii and of all intrinsic $V-I_C$ color), the mean value of $\Delta(I_C-K)$ is 0.36 mag (with a standard deviation of 0.72 mag) and the median value is 0.26 mag. In other words, despite all of the effects that can act to reduce the magnitude of the near-infrared excess—photometric variability, spectral type errors, and inner disk holes—*the average ONC star has a* 2 μm *excess* $\gtrsim$0.3 mag. We show the distribution of $\Delta(I_C-K)$ in Figure 9, with dotted lines indicating the $\Delta(I_C-K)$'s for no infrared excess and the mean infrared excess for the entire ONC sample.

We remind the reader of the results in § 3.2 that demonstrate that the magnitude of $\Delta(I_C-K)$—and thus our ability to diagnose the presence of disks—is a function of (1) the effective temperature/mass of the central star, (2) the radius of the central star, (3) the mass-accretion rate through the circumstellar disk, (4) the inclination of the star/disk system, and (5) the presence/absence of a magnetospheric "disk hole" and its size. K-band excesses generally increase for (1) stars of higher effective temperature/mass, (2) stars of smaller radius (at constant temperature), (3) star/disk systems of higher disk accretion rate, (4) system inclinations nearer pole-on than equator-on, and (5) as magnetospheric holes decrease in size (see Fig. 7). In the ONC, yet another factor may influence the observed K-band excess: location within the cluster. The ONC appears to show evidence for both mass segregation and age segregation (Hillenbrand 1997). If, as we believe from the disk models, there are systematic effects in the magnitude of the infrared excess with stellar mass and age, these may be reflected in systematic trends with projected cluster radius. Furthermore, the ONC stellar density falls off in a manner consistent with lowered isothermal sphere models (Hillenbrand & Hartmann 1998). In the central regions of the Trapezium, where the mean separation between stars is only a few thousand AU, tidal interactions between star/disk systems passing within a few hundred AU of one another could in principle increase the disk accretion rate and thus the observed infrared excess (Ostriker 1994).

From Figure 8, there indeed are trends apparent in the magnitude of the infrared excess both as a function of stellar color/temperature/mass and as a function of projected cluster radius. As a function of $V-I_C$ color, the mean value of $\Delta(I_C-K)$ generally rises from the bluest stars to a peak around $V-I_C=1.75$ and then declines toward redder colors. Earlier type, higher mass stars ($V-I_C\lesssim 1$) have smaller mean 2 μm excesses than the average star, while later type, lower mass stars ($1\lesssim V-I_C\lesssim 2.5$) have mean 2 μm excesses distributed with mass roughly as expected from the disk models: stars of lower masses appear to have smaller excesses. As a function of projected cluster radius, the values of $\Delta(I_C-K)$ appear to increase toward the cluster center.

In Figures 10, 11, and 12 we illustrate these apparent trends more clearly by showing histograms of the measured $\Delta(I_C-K)$ values for stars located in different bins in stellar mass, stellar radius, and projected cluster radius.

We have restricted this investigation to stars with $M/M_\odot<1.5$ in order to minimize the dynamic range in stellar mass (particularly for the stellar radius plot) and stellar radius (particularly for the stellar mass plot) variables. There is a clear trend for the mean $\Delta(I_C-K)$ values to decrease with decreasing stellar mass and increasing stellar radius, which is consistent with what is expected from the disk models (§ 3.2). There also is a clear trend for the mean $\Delta(I_C-K)$ values to increase systematically toward the cluster center. This trend with projected cluster radius is the strongest of the three outlined here but the only one that is not predicted a priori.

The trends manifest in Figures 10, 11, and 12 probably reflect some *combination* of (1) the true frequency of stars surrounded by circumstellar disks, (2) the relative importance of various disk properties (e.g., accretion rate, inner disk hole size), and (3) the relative contrast between photospheric and disk emission. As was stated above, we expect the magnitude of the near-infrared excess for a star surrounded by a circumstellar disk, as measured by $\Delta(I_C-K)$, to be a function of stellar mass, stellar radius, system inclination, disk accretion rate, and inner disk hole size. We have demonstrated the dependency of the observable $[\Delta(I_C-K)]$ on stellar mass and radius in this section. In the following section we estimate the disk frequency, making some attempt to correct for our sensitivity to disks sur-

[4] Of note is that almost all (>90%) of the stars with negative values of $\Delta(I_C-K)$ were originally located in the $(V-I_C)$-(I_C-K) diagram within 0.1 mag of the dwarf locus. Thus the subtraction of almost any amount extinction from these stars leads to their location below the dwarf locus and produces a negative quantity for $\Delta(I_C-K)$. Careful review of these cases leads us to the conclusion that the $V-I_C$ colors are somehow measured as too red, and/or the I_C-K colors are somehow measured as too blue compared with what is expected from the spectral types of these stars. This phenomenon may be explainable if the intrinsic stellar colors for $\sim$1 Myr old stars are sufficiently different from those of dwarfs at the latest spectral types to produce negative values of $\Delta(I_C-K)$ using our methodology. Photometric variability may play some role as well.

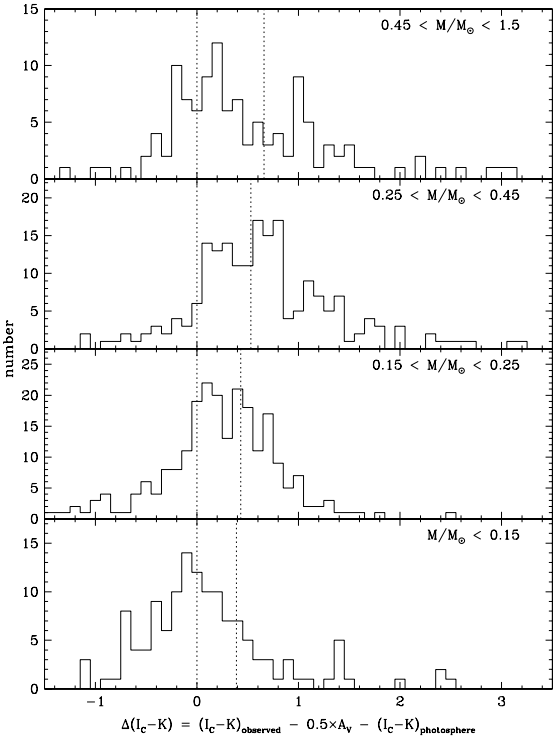

FIG. 10.—Histogram of near-infrared excesses as a function of stellar mass. Only stars less massive than 1.5 $M_\odot$ are shown. The magnitude of the infrared excess is larger for stars of higher mass, as is expected from the theoretical calculations presented in § 3.2. Vertical dotted lines indicate no excess [$\Delta(I_C-K)=0$] and the approximate excess expected from a pure-irradiation disk assuming a stellar radius of 2 $R_\odot$; stars with $\Delta(I_C-K) > \Delta(I_C-K)_{\rm irradiation}$ are candidate accretion disks.

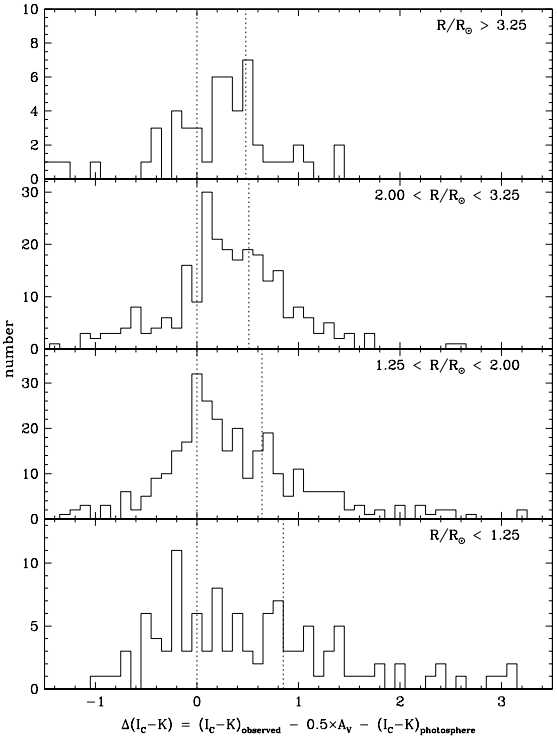

FIG. 11.—Histogram of near-infrared excesses as a function of stellar radius. Only stars less massive than 1.5 $M_\odot$ are shown. The magnitude of the infrared excess is larger for stars of smaller radius, as is expected from the theoretical calculations presented in § 3.2. Vertical dotted lines indicate no excess [$\Delta(I_C-K)=0$] and the approximate excess expected from a pure-irradiation disk assuming a stellar mass of 0.3 $M_\odot$; stars with $\Delta(I_C-K) > \Delta(I_C-K)_{\rm irradiation}$ are candidate accretion disks.

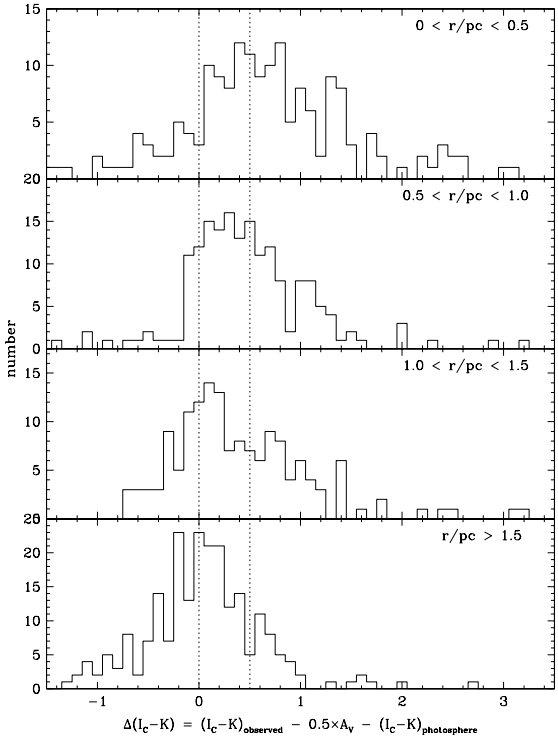

FIG. 12.—Histogram of near-infrared excesses as a function of projected cluster radius. Only stars less massive than 1.5 $M_\odot$ are shown. The magnitude of the infrared excess is larger for stars located closer to the cluster center. Vertical dotted lines indicate no excess [$\Delta(I_C-K)=0$] and the approximate excess expected from a pure-irradiation disk assuming a stellar mass of 0.3 $M_\odot$ and a stellar radius of 2 $R_\odot$; stars with $\Delta(I_C-K) > \Delta(I_C-K)_{\rm irradiation}$ are candidate accretion disks.

rounding stars of different mass and radius, taking inclination into account. Issues related to inner disk hole sizes and accretion rates unfortunately cannot be quantified from the present data. However, because these effects always act to reduce (inner holes) and to increase (accretion) the magnitude of the near-infrared excess, we can make some attempt to address their consequences.

5. THE DISK FREQUENCY

In this section we describe our methodology for quantifying the fraction of stars surrounded by disks. To study trends in the disk frequency, we first take the standard approach of counting the number of stars with near-infrared excesses larger than a specified limit as a fraction of the total number in our sample. We consider two different values for the limit an object must exceed in order to be labelled an infrared-excess star, $\Delta(I_C-K) > 0.1$ mag and $\Delta(I_C-K) > 0.3$ mag. Observational errors in determining $\Delta(I_C-K)$ toward lower mass stars (see Table 2) imply that the former of these limits could be considered too liberal in terms of admitting false infrared-excess candidates. The theoretically expected values of $\Delta(I_C-K)$ for disk surrounding lower mass stars [$\Delta(I_C-K)=0.2$ mag for an irradiation-dominated disk that extends all the way in to the dust sublimation point but that is inclined at the most likely value of 60°, surrounding an M6 star having 0.1 $M_\odot$ at the 1 Myr age of the ONC] imply that the latter of these limits could be considered too conservative in terms of excluding bona fide infrared-excess candidates. The consideration of both values for the limit in $\Delta(I_C-K)$ should

provide a reasonable estimate of the minimum disk fraction. The disk fractions estimated using this methodology are minima, since some stars with disks will have $\Delta(I_C-K)$ values less than our chosen limit because of the effects of inclination, inner disk holes, and low star/disk contrast. Furthermore, the disk fractions may be considered minima, since the errors in our $\Delta(I_C-K)$ diagnostic are primarily negative (see Table 2) except in cases where A_V is large.

Most previous estimates of disk fractions have been made on the basis of observed (that is, not corrected for the effects of reddening or for the stellar photosphere) color-color diagrams. The only exception is for stars in the Taurus-Auriga cloud where studies have proceeded in a manner analogous to that outlined above, namely by defining a value of the intrinsic near-infrared excess above which stars are considered to be surrounded by disks and below which they are considered to lack disks. Because of the much larger range in mass represented by stars in the ONC, based on the results of § 3.2, we argue that a similar approach here would be naive. Stellar mass, stellar radius, and disk accretion rate driven changes in the "contrast" between disk and photospheric emission and the unknown effects of inclination of the star/disk system and inner disk hole size *are* important. Thus the value one calculates for the number of stars having near-infrared excess as a fraction of the total depends on the range in stellar radius (age) and stellar mass represented by the population, as well as on the distributions of inner disk hole sizes and disk accretion rates.

We can estimate and correct for the effects of both inclination and the stellar parameters, however, by determining from the pure-irradiation disk models the percentage of randomly oriented disks (as a function of stellar mass and age) to which we are sensitive using our two different limits in $\Delta(I_C-K)$. We calculate the inclination required to drive $\Delta(I_C-K)$ from its pole-on value to below our limiting value and then calculate the fraction of any randomly oriented sample of star/disk systems with inclination angles in excess of the critical value. We can then correct the apparent disk frequency upward by the appropriate percentage. The disk fractions derived using this more sophisticated methodology are maxima, since some disks will have $\Delta(I_C-K)$ larger than the value expected from randomly oriented pure-irradiation disks because of the effects of accretion. In particular, corrected disk fractions larger than unity are possible and imply that we detect more disks than expected under the assumption of pure irradiation disks seen over a random distribution of inclination angles, i.e., that the infrared excesses are larger than those produced by passive disks and so that the disks are accreting.[5]

Averaging over all stellar masses, stellar ages, and projected cluster radii, we derive a lower limit to the overall disk frequency in the ONC as 55%. This is the average of the fraction of stars with $\Delta(I_C-K) > 0.1$ mag and those with $\Delta(I_C-K) > 0.3$ mag. By correcting the value of 55% upward by the factors appropriate for a star having the mean stellar mass (0.8 $M_\odot$), the mean stellar age (0.8 Myr), and located at the half-mass radius (0.8 pc) of the cluster, we derive an upper limit to the overall disk frequency of 90%.

[5] We have assumed in the above that the effects of inner disk holes are negligible. If a certain fraction of our sample does have inner disk holes of size sufficient to drive $\Delta(I_C-K)$ below detectable limits, both our "lower limit disk fraction" and our "upper limit disk fraction" will in fact be lower limits.

We subdivide the sample into bins in stellar mass, stellar age, and projected cluster radius in § 6 and look for trends in the apparent disk fractions and the corrected disk fractions with these variables.

6. TRENDS IN DISK FREQUENCY WITH STELLAR PROPERTIES AND CLUSTER ENVIRONMENT

In this section we explore trends in the disk frequency with stellar age, stellar mass, and projected cluster radius. We consider first the full population of stars for which disks can be detected. However, with knowledge of the large array of influences on the observed infrared excess, quantifying the disk frequency as a function of stellar age, stellar mass, and cluster environment requires careful parsing of our sample in order to separate and understand the effects of multiple parameters affecting our disk diagnostic. When any trends are apparent, their robustness must be examined in light of all these systematic effects. Because of the possibility that some of the trends apparent in the disk frequency with age, mass, and cluster radius could be artifacts of other trends between the same variables (i.e., not necessarily related to the disks), we must be careful to isolate each variable of interest from any possible influences by the others. We thus make use of subsamples of stars restricted to particular ranges in age, mass, or cluster radius, in addition to the full samples.

6.1. *Stellar Age*

The constraint on disk lifetimes derived by examining the disk fraction as a function of time provides an empirical limit on the duration of the disk accretion phase, which is critical for understanding: the evolutionary paths followed by pre–main-sequence stars in the HR diagram, their ultimate masses, their angular momentum histories, and the timescales available for planetesimal building. Stars in the ONC span only a limited range in age (>80% of the stellar population is <1 Myr old), and thus we expect relatively little disk evolution, since *typical* lifetimes for disks surrounding solar-type stars appear to be in the range 3–10 Myr (Skrutskie et al. 1990; Allen 1996). However, if in the ONC the disk accretion rates are or were high enough, disk evolutionary timescales could be short enough to produce discernible differences between stars in their infrared excess characteristics, even at such young ages. Is there a correlation of the disk fraction with stellar age?

In Figure 13 we present, as a function of stellar age, the disk frequency calculated using our two different limits for disk detection, 0.1 and 0.3 mag in $\Delta(I_C-K)$. We use the theoretical pre–main-sequence evolutionary calculations of D'Antona & Mazzitelli (1994) to derive stellar ages and include only stars less massive than 1.5 $M_\odot$ in these plots so as to reduce the mass-dependent effects of the stellar birthline, which is not incorporated in the D'Antona & Mazzitelli (1994) calculations. In the upper panel we show the apparent disk fraction, that is, as calculated from the data with no corrections for sensitivity as a function of disk inclination or stellar age. At 0.8 Myr (the mean age), we infer a lower limit to the true disk fraction of ~65%. There is little evidence for the expected decrease in disk frequency with increasing age, even when only a particular range of stellar masses or projected cluster radii is considered (see Fig. 13). If anything, there appears to be a drop in the upper panel of the apparent disk frequency toward *younger* stars. As we now demonstrate, however, this is the result of decreasing

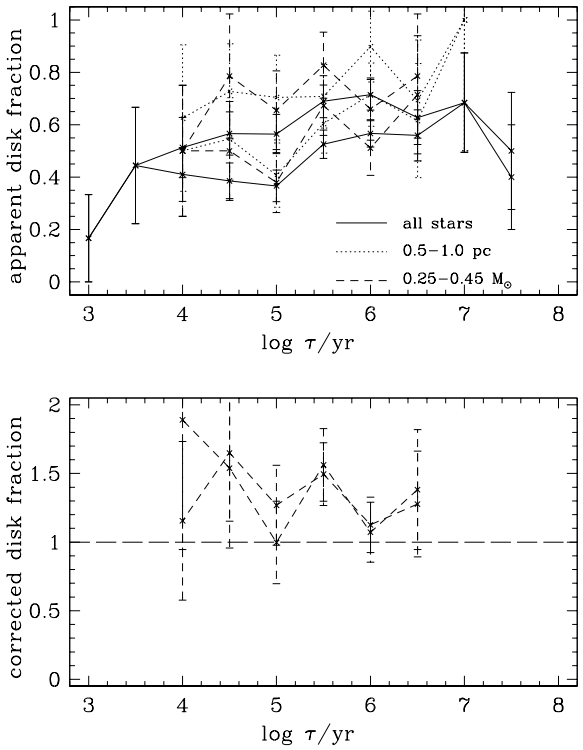

FIG. 13.—Variation of apparent disk frequency (*upper panel*) and the corrected disk frequency (*lower panel*) with stellar age. Only stars less massive than 1.5 $M_\odot$ are included to reduce the effects of the stellar birthline. In the upper panel, disk fraction is calculated for each age bin as the number of stars with $\Delta(I_C-K) > 0.3$ mag (*lower lines*) and greater than 0.1 mag (*upper lines*) over the total number of stars. The solid lines indicate all stars in our sample, while the dashed lines indicate stars over a restricted mass range just above the peak of the mass function, 0.25–0.45 $M_\odot$, and dotted lines indicate stars over a restricted radial range around the half-mass radius of the cluster, 0.5–1.0 pc. Only bins with more than 3 points in them are plotted; error bars reflect Poisson statistics. The full and restricted samples show the same trend in the disk frequency with stellar age. In the lower panel, the apparent disk fraction for 0.25–0.45 $M_\odot$ stars has been corrected for inclination effects as described in the text. A disk fraction larger than unity (*horizontal dashed line*) demonstrates that these disks are accretion disks (see § 5). There is little evidence for any trend in the disk frequency with stellar age, at least over the limited range of ages in the ONC; the decrease in the apparent disk fraction for the youngest ages is probably a consequence of decreasing star/disk contrast for larger (younger) stars.

star/disk contrast toward larger stellar radii. In the lower panel we show the apparent disk frequency corrected for the effects of inclination and for the relative contrast as a function of stellar age. The correction factors were derived by calculating, at constant mass, an age-radius relationship from the theoretical isochrones of D'Antona & Mazzitelli (1994) and then deriving from the model expectations for pure-irradiation disks surrounding stars of different radii, the inclination to which we are sensitive using the 0.1 and 0.3 mag limits in $\Delta(I_C-K)$, as described above. The correction factors we divide by at a mass of 0.35 $M_\odot$, using a limit in $\Delta(I_C-K)$ of 0.1 mag, range from 0.43 at an age of 10^4 yr to 0.62 at an age of 3×10^6 yr. Of note is that the disk frequency derived by making corrections to the 0.1 mag limit in $\Delta(I_C-K)$ is nearly identical to that derived by making corrections to the 0.3 mag limit in $\Delta(I_C-K)$, as shown in the lower panel of Figure 13. This suggests that the differences between using the 0.1 and the 0.3 mag limit to derive the apparent disk frequency (*upper panel* of Fig. 13) are driven primarily by the effects of inclination.

In summary, even when proper accounting is made for our relative sensitivity to circumstellar disk detection as a function of stellar age and disk inclination, no evidence is found for evolution of the disk frequency with time. Without consideration of the effects of accretion, an upper limit to the disk fraction at the mean age of the cluster (0.8 Myr) is 100% while the lower limit is 65%. We note that the sample considered here is composed of stars less than 1.5 $M_\odot$ in order to reduce the effects of the stellar birthline that has not been included in the calculations of pre–main-sequence isochrones.

Finally, we note that there are large theoretical uncertainties in stellar ages at such extremely early evolutionary stages.

6.2. *Stellar Mass*

The large mass range (<0.1–50 $M_\odot$) in the ONC combined with its small age range (<1 Myr) strongly suggests that in order for this ensemble of stars to have individually assembled on a coherent timescale, the time-averaged rate of mass accumulation must be higher for the higher mass stars than it is for the lower mass stars. However, it is not clear at present whether, during star formation, the bulk of the total mass accretion takes place during the initial infall of a spherical or flattened protostellar envelope, through steady disk accretion after the star is optically revealed, or through episodic phases of elevated disk accretion. Current arguments regarding the accretion rates and the survival times of circumstellar disks surrounding stars of different mass come from piecing together information obtained for samples of stars in different star-forming regions usually spanning different mass (and sometimes age) ranges. The ONC database, by contrast, allows us to look for direct evidence of differences in the evolutionary timescales for disks surrounding stars of different mass in a single extremely young population. Is there a correlation of the disk fraction with stellar mass?

In Figure 14 we present, as a function of stellar mass, the disk frequency calculated using our two different limits for disk detection, 0.1 and 0.3 mag in $\Delta(I_C-K)$. We use the theoretical pre–main-sequence evolutionary calculations of D'Antona & Mazzitelli (1994) to derive stellar masses. In the upper panel we show the apparent disk fraction, that is, as calculated from the data with no corrections for sensitivity as a function of disk inclination or stellar mass. At 0.8 $M_\odot$ (the mean mass), we infer a lower limit to the true disk fraction of $\sim 55\%$; there is some evidence for a general decrease in the disk frequency toward higher stellar masses, even when only a particular range of stellar ages or projected cluster radii is considered (see Fig. 14). There is also an indication of a decrease in the disk frequency toward the lowest stellar masses. The latter trend, however, may be the result of decreasing star/disk contrast toward lower stellar masses. To investigate this possibility we show in the lower panel the apparent disk frequency corrected for the effects of inclination and for the relative contrast as a function of stellar mass. The correction factors were derived by calculating from the model expectations for pure-irradiation disks surrounding stars of different mass the inclination to which we are sensitive using the 0.1 and 0.3 mag limits in $\Delta(I_C-K)$, as was described above. The correction factors we divide by at an age of 1 Myr using a limit in $\Delta(I_C-K)$ of 0.1 mag range from 0.47 at a mass of 0.1 $M_\odot$ to 0.61 at a mass of 1.0 $M_\odot$ to 0.79 at a mass of 5.0 $M_\odot$. The so-corrected

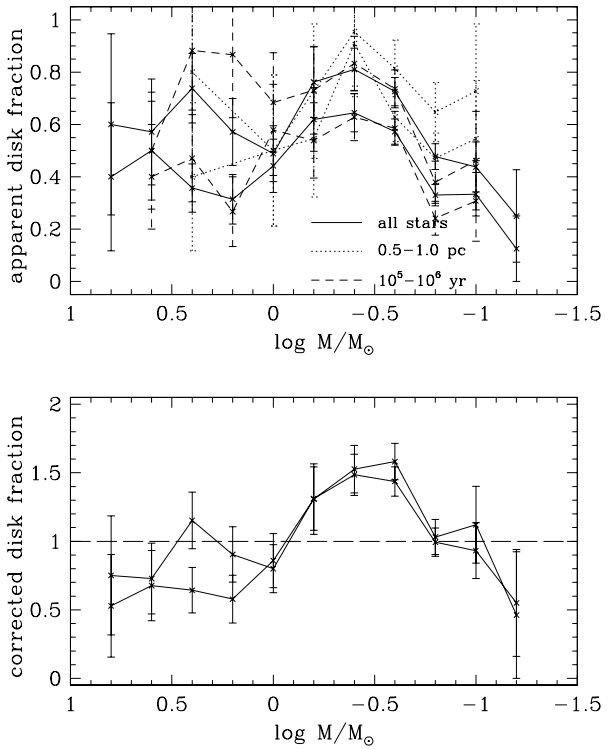

FIG. 14.—Variation of the apparent disk frequency (*upper panel*) and the corrected disk frequency (*lower panel*) with stellar mass. In the upper panel, disk fraction is calculated for each mass bin as the number of stars with $\Delta(I_C-K) > 0.3$ mag (*lower lines*) and greater than 0.1 mag (*upper lines*) over the total number of stars. The solid lines indicate all stars in our sample, while the dashed lines indicate stars over a restricted age range, 10^5–10^6 yr, and dotted lines indicate stars over a restricted radial range around the half-mass radius of the cluster, 0.5–1.0 pc. Only bins with more than 3 points in them are plotted; error bars reflect Poisson statistics. The full and restricted samples show the same trend in the disk frequency with stellar mass. In the lower panel, the apparent disk fraction for the full sample has been corrected for inclination effects as described in the text. A disk fraction larger than unity (*horizontal dashed line*) in this plot demonstrates that these disks are accretion disks (see § 5). There is a clear trend of increasing disk frequency toward lower mass stars, except for the lowest mass stars where the disk frequency starts to decline.

disk fraction is then sensitive only to the effects of accretion and of inner disk holes. If the disks are accreting, then we may overestimate the disk fraction. If the disks have inner disk holes, then we may underestimate the disk fraction. We note, however, that even the presence of inner disk holes of the nature discussed by Hillenbrand et al. (1992) for Herbig Ae/Be stars would not render the disks around higher mass stars undetectable at 2 μm. As was found in our discussion of stellar ages, the disk frequency derived by making corrections to the 0.1 mag limit in $\Delta(I_C-K)$ is nearly identical to that derived by making corrections to the 0.3 mag limit in $\Delta(I_C-K)$, as is shown in the lower panel of Figure 14. This suggests that the differences between using the 0.1 and the 0.3 mag limit to derive the apparent disk frequency (*upper panel*, Fig. 14) are driven primarily by the effects of inclination.

In summary, from both the apparent disk frequency and the corrected disk frequency in which proper accounting is made for our relative sensitivity to circumstellar disk detection as a function of stellar mass and disk inclination, we find evidence for a falloff in the disk fraction toward higher stellar masses from $\sim$0.3 to $\sim$5 $M_\odot$. Above 5 $M_\odot$ where the statistics are poor (there are only 13 stars with masses 5–50 $M_\odot$), we find that while about $\frac{1}{2}$ of these stars do have near-infrared excesses at the level of $\lesssim$0.2 mag, their spectral energy distributions are consistent with the excesses expected from free-free emission or from optically thin dust and *not* with the optically thick, dusty (accretion) disks that are present around lower mass stars in the ONC. We also find evidence for falloff in the disk frequency at the lowest stellar mass ($\lesssim$0.2 $M_\odot$); the robustness of this trend is discussed further in § 6.4. Without consideration of the effects of disk accretion, an upper limit to the disk frequency at the mean stellar mass (0.8 $M_\odot$) is 90%, while the lower limit is 55%. If the ONC is indeed close to being "coeval," then the high fraction of disks around low-mass stars combined with the relative lack of disks around the highest mass stars suggests that the higher mass stars have dissipated their disks more quickly, perhaps because the characteristic accretion rates for higher mass systems are higher.

6.3. *Projected Cluster Radius*

In regions such as the inner portion of the ONC where the mean distance between stars is only $\sim$1000 AU or 5–10 times the size thought characteristic of circumstellar disks, environmental factors such as the enhancement of accretion rates or the tidal truncation of disks may be important. The resultant shortening of circumstellar disk lifetimes might produce a preferential absence of disked stars in the innermost cluster regions. Another reason to suspect a possible absence of disks toward smaller cluster radii is the enhanced UV radiation field in the inner cluster that has been posited to destroy disks (Hollenbach et al. 1994). Does the disk fraction change as a function of distance from the Trapezium stars?

In Figure 15 we present, as a function of projected cluster radius, the disk frequency calculated using our two different limits for disk detection, 0.1 and 0.3 mag in $\Delta(I_C-K)$. In the upper panel we show the apparent disk fraction, as calculated directly from the data, and find a general decrease in the disk frequency toward the outer cluster regime, even when only a particular range of stellar ages or stellar masses is considered. This trend may, however, be the result of decreasing cluster membership probability toward the outer cluster. To investigate this possibility, we show in the lower panel the apparent disk frequency corrected for the relative membership probability (97%, 97%, 89%, 80%, 68%, and 50% for 0.5 pc radial bins ranging from 0 to 3 pc) derived in the study of Jones & Walker (1988) and for the effects of inclination assuming the mean mass and age of the cluster. We note that the membership corrections are likely to be overestimates, since our spectroscopic sample is heavily biased toward proper motion members. Only 6% of the spectroscopic sample are known nonmembers; removing these stars from the top panel of Figure 15 has no effect. Because there are no systematic effects in our ability to detect disks from near-infrared excesses as a function of cluster radius, we interpret the trend of higher disk frequency in the inner cluster to be a real indicator of differences in the circumstellar disk properties as a function of cluster radius. As is notably different than we found from investigation of the trends in disk frequency with stellar age and stellar mass, with projected cluster radius the disk frequency derived by making corrections to the 0.1 mag limit in $\Delta(I_C-K)$ is not the same as that derived by making corrections to the 0.3 mag limit in $\Delta(I_C-K)$. This suggests that the differences in the apparent disk frequency illus-

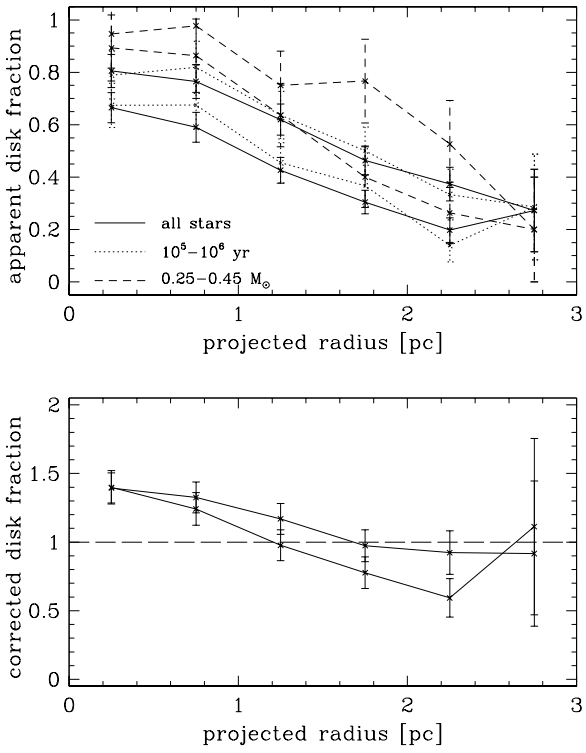

FIG. 15.—Variation of apparent disk frequency (*upper panel*) and corrected disk frequency (*lower panel*) with projected cluster radius. In the upper panel, disk fraction is calculated for each radial bin as the number of stars with $\Delta(I_C-K) > 0.3$ mag (*lower lines*) and greater than 0.1 mag (*upper lines*) over the total number of stars. The solid line indicate all stars in our sample, while the dashed lines indicate stars over a restricted mass range just above the peak of the mass function, 0.25–0.45 $M_\odot$, and dotted lines indicate stars over a restricted age range, 10^5–10^6 yr. The full and restricted samples show the same trend in the disk frequency with projected cluster radius, that is, a steady decline from the inner to the outer cluster regions. This figure also illustrates our finding that stars in the mass range 0.25–0.45 $M_\odot$ are more likely to have disks than the average star whose mass is $\sim$0.8 $M_\odot$. In the lower panel, the apparent disk fraction for the full sample has been corrected for contamination by nonmembers as described in the text. A disk fraction larger than unity (*horizontal dashed line*) in this plot demonstrates that these disks are accretion disks (see § 5).

trated in the upper panel of Figure 15 are real, i.e., they are *not* explainable by inclination effects. A possible cause of this discrepancy is differences in the disk accretion rates with cluster radius.

In summary, we find evidence for a general falloff in the disk frequency with increasing projected cluster radius. We suggest that the rise in the disk fraction toward the inner cluster regions may be caused by enhanced disk detectability driven by an increase, over the radial average, in the disk accretion rates toward the cluster center. Based on other characteristics of the inner ONC regions, we suggest that enhanced accretion activity may be an effect of younger stellar ages, higher stellar masses, higher stellar densities, or combinations of these. Most significantly, there is no evidence for a *decrease* in the fraction of stars surrounded by disks in the central cluster regions, indicating that photoevaporative effects have not yet had time to destroy the inner disks.

6.4. *Summary and Discussion of ONC Disk Trends*

In the previous subsections we have made use of near-infrared excess emission to search for systematic trends in disk frequency as a function of stellar age, stellar mass, and the location of a star-disk system within the ONC. Our strategy has been to use the quantity $\Delta(I_C-K)$ as our primary indicator of the presence/absence of a disk. However, the effects of modest inner disk holes and high inclination may in some cases preclude detection of significant near-infrared excess emission arising from disks, leading to misclassification of star/disk systems as possible diskless objects. The apparent disk fractions must thus be considered *lower limits* to the true fraction of stars surrounded by circumstellar accretion disks. We have attempted to correct the apparent disk frequency for the effects of inclination as a function of stellar age and mass. However, the so-called corrected disk fractions must be considered *upper limits* to the true fraction of stars surrounded by circumstellar accretion disks, since they assume that all disks are pure-irradiation disks and thus do not take accretion into account. The presence of accretional heating large enough to exceed the irradiative heating can produce a corrected disk frequency larger than unity. Based on our data, we constrain the overall disk frequency in the ONC (averaged over all stellar masses, stellar ages, and projected cluster radii) to be between $\sim$55% and $\sim$90%. The former value is that observed as the average disk fraction from our $\Delta(I_C-K)$ diagnostic, while the later value comes from correcting the observed value upward by the factors described in previous subsections appropriate for a star having the mean stellar mass (0.8 $M_\odot$), the mean stellar age (0.8 Myr), and located at the half-mass radius (0.8 pc) of the cluster. We summarize our findings on the trends in disk frequency with stellar age, stellar mass, and projected cluster radius in Table 3.

Attempts to correlate the disk fraction with stellar age suggest that over the age range $\lesssim$0.1–2 Myr there is no differentiation of the near-infrared excess fraction with stellar age. Owing both to the effects of accretion (which clears disks of material) and to the possible effects of planet building (which reduces the optical depth of disks owing to grain agglomeration), we do expect the fraction of stars that exhibit near-infrared disk signatures to decrease with age. The large sample of stars spanning masses from less than 0.1–50 $M_\odot$ in principle make the ONC an ideal laboratory for quantifying the evolution of disks at early evolutionary phases. However, the extreme youth of the ONC appears to render difficult the detection any direct evidence for the evolution of inner circumstellar disks.

Attempts to correlate the disk fraction with stellar mass suggest that more massive stars are less likely to have near-infrared excesses than are lower mass stars. This result is robust given the large values of $\Delta(I_C-K)$ expected even for completely passive disks surrounding stars of spectral types A and earlier. The lack of disk signatures among the most massive stars ($M > 5$ $M_\odot$) combined with the high disk frequency among stars with masses $\sim$0.2–5 $M_\odot$ seems best explained by a difference in average disk lifetimes. Disk evolutionary times around higher mass stars must be shorter if stars of all masses in the ONC formed nearly simultaneously (within $\sim$1 Myr). This is consistent with higher accretion rates and, subsequently, more rapid evolutionary times, on average, for disks surrounding higher mass stars.

However, there is also a noticeable lack of evidence for disks surrounding many of the lowest mass ($M \lesssim 0.2$ $M_\odot$) stars compared with those in the mass range $0.2 \lesssim M/M_\odot \lesssim 1.0$. We show the detailed mass distributions for stars with and without evidence of near-infrared excess in

TABLE 3

DISK FREQUENCY FROM $\Delta(I_C-K)$ IN THE ONC

Parameter	% (observed and corrected)	⟨%⟩
With Stellar Age		
log τ/yr:		
4	45–100	73
5	50–100	75
6	65–100	83
7	70–90	80
With Stellar Mass		
log $M/M_\odot$:		
−1.2	20–50	35
−1.0	40–100	70
−0.8	45–100	73
−0.6	65–100	83
−0.4	75–100	88
−0.2	70–100	85
0.0	50–80	65
0.2	45–75	60
0.4	55–80	68
0.6	50–70	60
0.8	50–65	58
1.0	0	0
1.2	0	0
1.4	0	0
1.6	0	0
With Cluster Radius		
r/pc:		
<0.5	75–100	88
0.5–1.0	70–100	85
1.0–1.5	55–100	78
1.5–2.0	40–100	65
2.0–2.5	30–100	55
2.5–3.0	30–100	65

Figure 16*a*. The median mass of the population with apparent near-infrared excess is higher than the median mass of the overall population, with the fraction of stars with detectable disks beginning to decrease below $\sim 0.2\ M_\odot$. Stars (and even candidate substellar objects) of all masses *can* have disks; it is the *frequency* of disks that appears lower for the lowest mass stars. This may be due to a combination of low disk accretion rates *and* moderate-sized inner disk holes, which is possibly sufficient for removal of *all* of the 2 μm excess in the lowest mass stars, as discussed in § 3.2. However, our similarly motivated investigation of the mass distributions of stars with broad Ca II triplet emission (§ 7.2) and of stars that have been designated as "externally ionized" (see § 7.3)—samples of stars that surely possess circumstellar disks—show the same trends, as is illustrated in Figures 16*b* and 16*c*. If the presence of Ca II triplet emission and of features associated with external ionization are independent of the inner disk characteristics measured by $\Delta(I_C-K)$, it would be unlikely for the effect with mass seen in all three of these diagnostics to be due solely to the effects of inner disk holes. If real, a lack of near-infrared excess associated with the lowest mass stars might be expected if disk accretion is relatively less important in forming the lowest mass stars than it is in forming all higher mass stars. In other words, if during the initial stages of protostellar collapse a star of mass $0.2\ M_\odot$ or less can form directly from infall of low angular momentum material onto a central object, while a star of greater mass forms from the same central seed mass plus the accretion of higher angular momentum material initially deposited in a disk, the

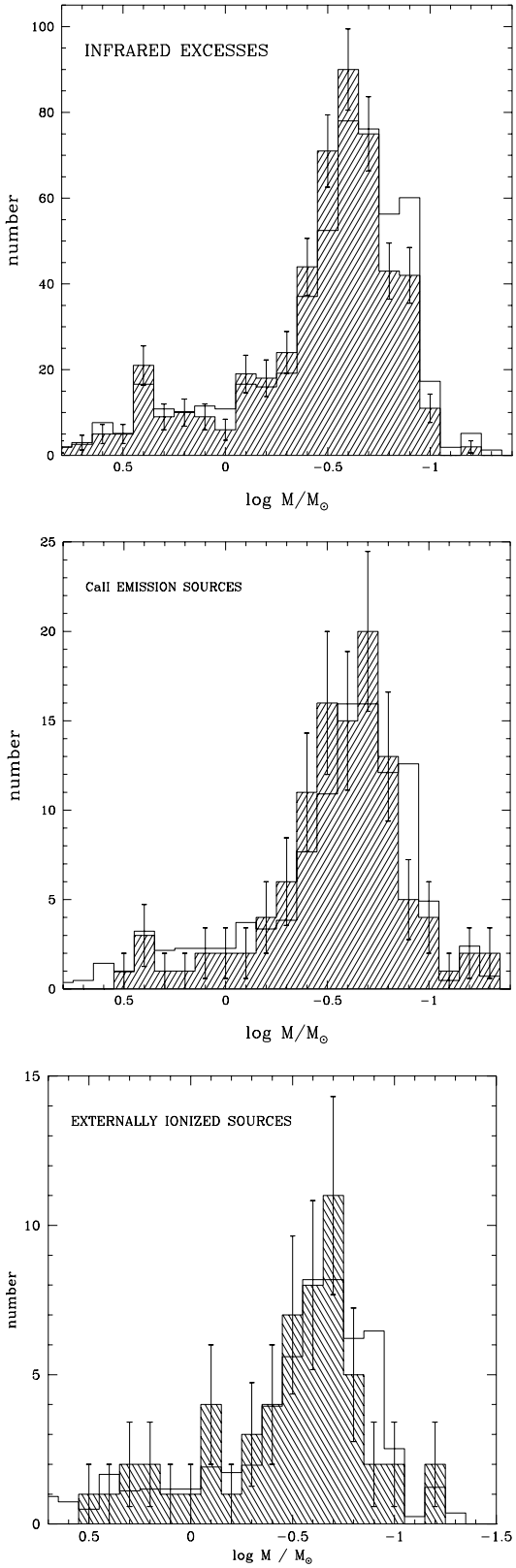

FIG. 16.—Distribution of stellar masses for (*open histogram in each panel*) the full ONC spectroscopic sample compared with (*upper panel*) stars with at least 0.1 mag of (I_C-K) excess, (*middle panel*) stars with Ca II triplet emission, and (*lower panel*) stars identified as being externally ionized. The total spectroscopic sample in each panel has been scaled in each case by the ratio of the sample sizes. The mass distribution for the infrared-excess sample appears underrepresented at the lowest masses compared with the mass distribution for the overall sample. The mass distributions for the Ca II and the externally ionized samples also appear underrepresented at the lowest masses compared with the mass distribution for the overall sample. Error bars represent counting statistics.

observed trend might be expected. Alternately, it may be that disks surrounding lower mass stars are smaller than those surrounding slightly higher mass stars and thus can dissipate on shorter timescales given the same accretion rates. A final possibility is that the lowest mass stars somehow have had their disks preferentially stripped in the high-density environment of the ONC. It is likely that only by obtaining longer wavelength photometry ($\gtrsim 3.5$ μm) will we be able to distinguish among these possibilities for the *apparent* lack of near-infrared excess associated with many of the lowest mass stars in the ONC.

Attempts to correlate the disk fraction with projected cluster radius produce a clear trend of decreasing disk fraction with increasing distance from the cluster center, even when we correct for the empirically determined radial falloff in cluster membership probability. We suggest that this trend arises from a systematic decrease in the mean disk accretion rate with increasing cluster radius, which reduces the contribution of the disk relative to photospheric emission thus making the infrared excess fall below our detection limit. We also note that despite the high stellar density and the intense UV radiation field, circumstellar disks do not appear to be completely destroyed in the inner cluster.

In evaluating the significance of these conclusions, we remind the reader that the contrast between disk and photospheric emission as measured by the observed near-infrared excess—and thus our ability to diagnose the presence of a disk—depends on many parameters: stellar mass and radius, system inclination, disk accretion rate, and the size of any inner disk hole. Our data set indeed reveals many of the systematic trends in disk/photosphere contrast expected from model calculations (see § 4). The quoted lower and upper bounds to disk fractions explicitly take into account the effects of stellar parameters and system inclination on disk detectability. However, we emphasize that we are unable to derive accurate accretion rates for our sample and that we have no means of estimating inner disk hole sizes from the data at hand. Hence, our results must be viewed with appropriate caution. More robust estimates of disk fractions and their systematics await longer wavelength infrared photometry that is less sensitive to the effects of star/disk contrast because of the much slower falloff with wavelength of disk emission—$\lambda F_\lambda \sim \lambda^{-4/3}$, compared with photospheric emission, $\lambda F_\lambda \sim \lambda^{-3}$—and to the effects of (small) inner disk holes.

7. EVIDENCE FOR ACCRETION

Thus far we have discussed the evidence for and the frequency of circumstellar disks associated with members of the ONC population using the near-infrared continuum excess as a diagnostic. In this section we consider the evidence that these disks are *accretion disks*. Available to us in this exercise are: the magnitude of the infrared excess, the presence of optical emission lines, and the designation of a source as a "proplyd."

7.1. *Near-Infrared Excess above the Expectations from Pure-Irradiation Disk Models*

As we discussed in § 3.2, the magnitude of the near-infrared excess is expected to be larger for more rapidly accreting disks. Considering the distribution of $\Delta(I_C-K)$ values in Figure 8, we conclude not only that a large fraction (55%–90%) of the stars in our sample have circumstellar disks, but also that *at least* 34% of the total sample and *at least* 61% of the disked sample have *accretion disks*. Of the 813 stars in Figure 8, 275 have values of $\Delta(I_C-K)$ above the expectations for pure-irradiation disks, suggesting an additional source of near-infrared flux that we attribute to accretion.[6] The $\Delta(I_C-K)$ values appear large enough to suggest disk accretion rates in the range 10^{-9}–10^{-6} $M_\odot$ yr^{-1}.

In the Taurus-Auriga dark cloud, Hartigan, Edwards, & Ghandour (1995) found that *all* stars with detectable near-infrared ($K-L$) continuum excesses also show the strong optical continuum excesses that are attributed to accretion; in other words, if a star shows some evidence in the near-infrared for a circumstellar disk, that disk is likely to be an accretion disk. Gullbring et al. (1998) conclude that the median value of the mass-accretion rate for this population of ~ 1 Myr stars is $\sim 10^{-8}$ $M_\odot$ yr^{-1}. To place more quantitative estimates on the distribution of disk accretion rates in the ONC we need to calibrate our $\Delta(I_C-K)$ index against $\dot{M}_{\rm acc}$. This involves calculating the accretion luminosity and then converting to an accretion rate using the appropriate stellar parameters and assuming an accretion geometry. In the absence of such a calibration, we estimate the mean accretion rate implied for our ONC sample by scaling from what is known for stars in Taurus.

We can identify as candidate accretion disks only those systems whose combination of disk accretion, system inclination, inner disk hole size, stellar mass, and stellar radius produce $\Delta(I_C-K)$ values in excess of what is predicted for a pole-on pure-irradiation disk. While more than 55% of the ONC sample have $\Delta(I_C-K) > 0$, only greater than 61% of these stars also have $\Delta(I_C-K)$ values above the expectations for a pole-on pure-irradiation disk. In Taurus, of the 35 stars with values of $\dot{M}_{\rm acc}$ given in Hartmann et al. (1998) and spectral types and V-, I-, K-band photometry given in Kenyon & Hartmann (1995), two have $\Delta(I_C-K) < 0$ and nine more have $\Delta(I_C-K)$ insufficient to render them detectable as accretion disk candidates. From the $\Delta(I_C-K)$ index, therefore, we would miss $\sim\frac{1}{3}$ of these stars in Taurus with accretion rates measurable from ultraviolet excess (either spectral veiling or photometric continuum excess). This implies that the ONC data are consistent with $\sim 88\%$ of the disked sample (or 50% of the total sample) having accretion disks, assuming a distribution of accretion rates like that found in the Taurus cloud. Put another way, assuming similar underlying accretion distributions in the ONC and Taurus, the mean accretion rate for the sample of ONC stars selected from the magnitude of $\Delta(I_C-K)$ is equivalent to that characterizing the upper $\frac{2}{3}$ of the Taurus sample, or $\log \dot{M}_{\rm acc} = -7.5$. Measurement of the lower envelope of the $\dot{M}_{\rm acc}$ distribution in either the ONC or Taurus requires a diagnostic more sensitive to low-$\dot{M}_{\rm acc}$'s than $\Delta(I_C-K)$, such as ultraviolet excess.

Near-infrared excess emission *can* provide a reliable indication of the presence/absence of accretion disks among

[6] It is of course possible to observe an infrared excess in a nonaccreting system that exceeds the expectations of the pole-on, no-hole reprocessing disk if the geometry of the circumstellar dust is highly flared or spherical instead of moderately flared and disklike. However, given that all ONC stars for which we can calculate the quantity $\Delta(I_C-K)$ have both optical/near-infrared photometry and spectral types, it is unlikely that these are envelope-dominated systems unless the emission at all optical/near-infrared wavelengths is dominated by scattered light components.

low-mass pre–main-sequence stars, except for particular combinations of small stellar masses, young stellar ages, low disk accretion rates, large inner disk holes, and high values of system inclination. We have argued in this subsection that $\sim$88% of the ONC stars with identifiable disks, and therefore $\sim$50% of the total ONC sample, have accretion disks. Establishing the presence or absence of accretion disks among *all* members of the stellar population of the ONC will require use of other diagnostics. We examine two supplemental accretion diagnostics available to us: the Ca II triplet in emission (§ 7.2) and externally ionized (a.k.a. "proplyd") nature (§ 7.3). We note that of the optical sources with the biggest near-infrared excesses [$\Delta(I_C-K) > 2$ mag] almost all are either Ca II emission-line sources or externally ionized.

7.2. Ca II *Triplet Emission*

In this section, we make use of the Ca II "infrared" triplet lines ($\lambda\lambda$8498, 8542, and 8662) to explore disk frequency among ONC stars with masses $M < 3\ M_\odot$ (the mass range where our new spectroscopic database is fully representative given that we did not reobserve any of the early-type stars with previously determined spectral types). The Ca II triplet was first studied in young stellar objects by Herbig & Soderblom (1980), who established from moderate resolution spectra that "classical" T Tauri stars exhibit strong Ca II triplet emission with relative strengths among the triplet lines differing sharply from the expected Gaunt factor values of 1:9:6, which is consistent with their formation in a region of high optical depth. Subsequent investigations (Hamann & Persson 1992; Batalha et al. 1996) at higher spectral resolution ($R > 10{,}000$) revealed that the triplet emission features exhibit both narrow ($\Delta v \ll 50$ km s^{-1}) and broad ($\Delta v \gg 100$ km s^{-1}) components. Batalha et al. (1996) show a convincing correlation for T Tauri stars of the broad component of the Ca II relative line fluxes (the narrow component shows a weaker correlation) with the spectral veiling measured at optical wavelengths. This trend is defined by both (1) a sample of stars that span a range in the veiling index (defined as the ratio of the total flux to the photospheric flux averaged over 5000–7000 Å) and (2) individual stars whose veiling index varies with time. However, not all stars that are veiled have broad Ca II emission, and not all stars that have broad Ca II emission are heavily veiled. Based on Figure 8 of Batalha et al. (1996), what *can* be concluded is that if the veiling index is $r \gtrsim 1.5$, the star should show broad Ca II emission, while if the veiling index is $r \lesssim 1.5$, the star usually does not (although may) show broad Ca II emission. The narrow component dominates among stars with relatively small veiling, $r \lesssim 0.5$. That the strength of both the broad and the narrow components of Ca II emission exhibit correlations with the veiling index implies correlation with the mass-accretion rate (Valenti, Basri, & Johns 1993; Hartigan et al. 1995; Gullbring et al. 1998).

Spectra over $\approx$5000–9000 Å at $\sim$5–8 Å per resolution element were obtained with several different telescopes and instruments, and are discussed more fully in Hillenbrand (1997). At this resolution ($\sim$230 km s^{-1}), the broad and narrow components of any Ca II emission are blended, both with one another and with the underlying photospheric absorption. Based on measurements of luminosity class *V* spectral standards, the strongest line of the triplet, λ8542, has an *absorption* equivalent width that is constant (to within 20%) from spectral type F2–K7 at $W(\lambda) \approx 3$ Å and decreases over the range K7–M5 from 3 to 1.5 Å. Based on the study by Batalha et al. (1996), to within 50%, the sum of the equivalent widths of the λ8542 broad and narrow *emission* components is -3 Å for classical T Tauri stars with spectral veiling $r \lesssim 0.5$; at r values 0.5–1.5, the emission equivalent width increases in rough proportion to r, while for $r > 1.5$ the emission equivalent width levels off at a few tens of angstroms (with higher values achieved in exceptional cases). Using the transformation between r and mass-accretion rate from Gullbring et al (1998), we infer that $W(\lambda 8542) \approx -3$ Å for $\dot{M}_{\rm acc} \lesssim 10^{-8}\ M_\odot$ yr^{-1} and increases significantly above this value only for stars with $\dot{M}_{\rm acc} > 10^{-7}\ M_\odot$ yr^{-1}. Hence, at our spectral resolution, low-mass ONC stars of age comparable with stars in Taurus-Auriga ($\tau \sim 1$ Myr), surrounded by accretion disks with mass-accretion rates $\dot{M}_{\rm acc} < 10^{-8}\ M_\odot$ yr^{-1}, should show "filled in" Ca II emission. [In other words, among such stars the observed equivalent width, $W(\lambda 8542)$, is expected to be 0 ± 1 Å.] Stars with higher accretion rates should exhibit detectable Ca II emission above continuum levels, while stars that lack accretion disks should show net Ca II absorption with absorption equivalent widths $W(\lambda 8542) > 1$ Å.

Given the above discussion, observations of the Ca II triplet in emission can in principle provide another, independent, estimate of the disk frequency. To calculate the spectroscopic (as opposed to photometric) disk frequency, we simply count the number of stars with $W(\lambda 8542) < 0$ Å as a fraction of the total number of stars in our spectroscopic sample. All measured values of $W(\lambda 8542)$ are listed in Table 1. For stars where neither emission nor absorption features were apparent from visual inspection, an equivalent width of "0" is listed. Our measurement uncertainty is estimated at ± 0.5 Å based on measurements of multiple spectra of the same star. We identify $\sim$20% (225 stars) of the spectroscopic sample to show clear evidence for broad (several hundred km s^{-1} FWHM) Ca II triplet emission. The ratio of emission-line strengths among the three components of the triplet varies from star to star in the ONC and is not always of near-equal flux, as has been found for T Tauri stars in the limited spectral type range represented in Taurus-Auriga. An additional $\sim$50% of the ONC sample that should have Ca II absorption lines (based on their spectral types as determined from other absorption lines) have these features partially or completely filled in. The remaining $\sim$30% (314 stars) have measured Ca II absorption. In summary, the spectroscopic disk frequency (averaged over all stellar ages, stellar masses, and projected cluster radii considered in this paper) is $\sim$70%. This value is to be compared with the similarly averaged *apparent* photometric disk frequency of $\gtrsim$55%, the corresponding *corrected* disk frequency of 90%, and the *accretion disk* frequency of $\sim$50% estimated in the previous subsection. The distribution of $\Delta(I_C-K)$ for those stars with Ca II emission is shown in Figure 9 (*hatched histogram*). Note that some of these stars have values of $\Delta(I_C-K)$ that are negative, underscoring our inability to detect *all* accretion disk systems using $\Delta(I_C-K)$ as a diagnostic.

Stars with Ca II triplet emission are represented among all masses ($\lesssim 0.1-3\ M_\odot$), ages ($\lesssim$0.1–2 Myr), and projected radii ($r < 3$ pc) in the ONC. Are the trends in disk frequency with stellar age, stellar mass, and projected cluster radius found using the photometric disk diagnostic, $\Delta(I_C-K)$, also apparent using the spectroscopic disk diag-

nostic, $W(\lambda 8542)$? An emission-line equivalent width suffers contrast effects with stellar mass and radius similar to those discussed in the context of the magnitude of the infrared excess. In particular, small emission-line equivalent widths are more difficult to detect for stars in the mass range where photospheric Ca II (and TiO) absorption is strongest. Small emission-line equivalent widths are also more difficult to detect around larger (younger) stars because of competition with the relatively larger surface area of the star. We do not attempt to correct for such effects (for example, by accounting for the underlying photospheric absorption and calculating line fluxes from the so-corrected equivalent widths). Instead, we simply present histograms of the measured Ca II $\lambda 8542$ line as a function of stellar age, stellar mass, and projected cluster radius in Figures 17, 18, and 19. These figures include stars with measured absorption, measured emission, and an arbitrarily assigned value of "0" equivalent width to all stars where the Ca II lines are filled in to the level of the continuum. As can be seen from these figures (comparable in nature to Figs. 10, 11, and 12), there are no clear trends in the distribution of Ca II equivalent widths with any of these three parameters. However, the *frequency* of Ca II emission—measured as the number of stars that exhibit clear Ca II emission summed with the number of stars with the Ca II lines filled in, the quantity divided by the total number of stars—is found generally to decrease toward older ages, higher masses, and larger projected cluster radii. These trends are similar to those suggested by the infrared data.

Examination of the subsample of stars with Ca II clearly in emission also suggests possible confirmation of the apparent decrease in disk fraction among the lowest mass stars in our sample inferred from $\Delta(I_C - K)$. Although the subsample of Ca II emission stars is completely representative of the ONC sample as a whole as judged from examination of the distribution of such stars in an H-R diagram, in Figure 16*b*, we find some indication that the detailed distribution of masses for the Ca II-emission stars differs

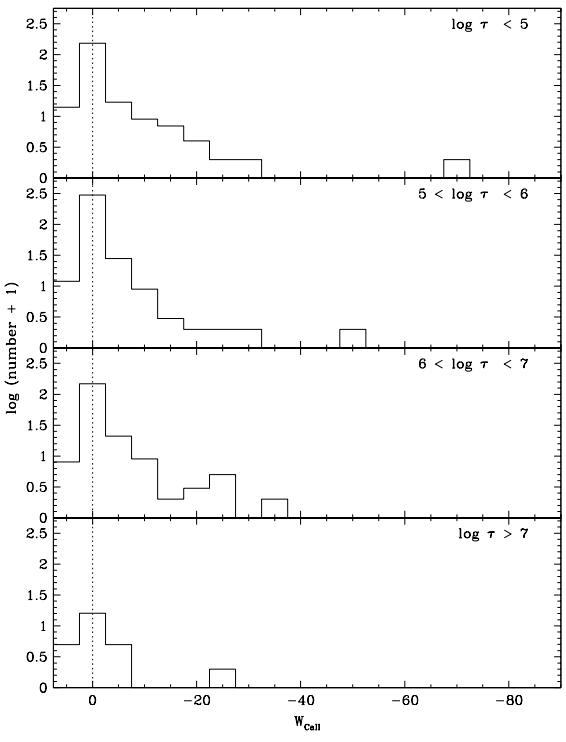

FIG. 17.—Distribution of Ca II $\lambda 8542$ equivalent widths with stellar age

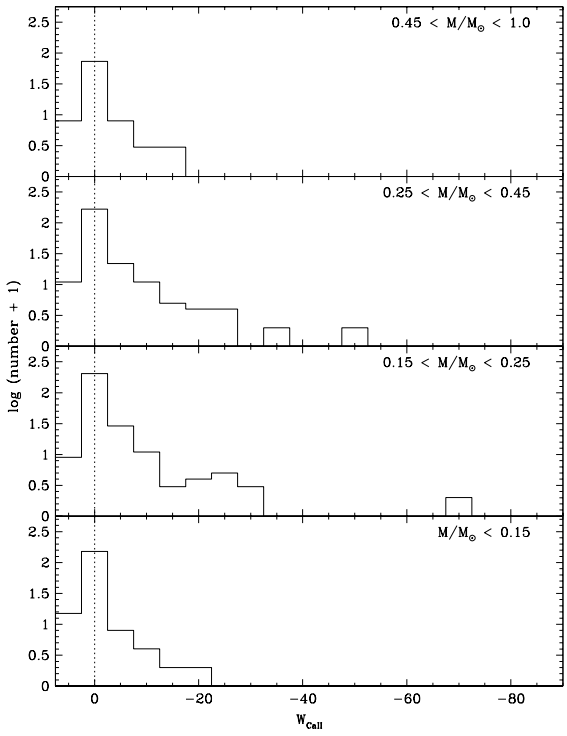

FIG. 18.—Distribution of Ca II $\lambda 8542$ equivalent widths with stellar mass

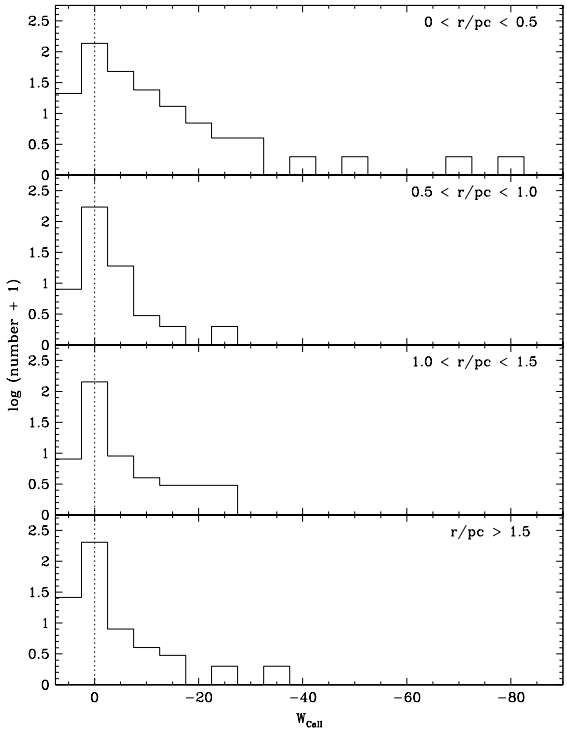

FIG. 19.—Distribution of Ca II $\lambda 8542$ equivalent widths with projected cluster radius.

from that found for the full spectroscopic sample: stars showing triplet emission peak at higher masses than those that lack such emission. We note, however, that while this result is consistent with a smaller disk fraction among the lowest mass stars, it could also reflect the effects of a systematic decrease of $\dot{M}_{\rm acc}$ with mass on Ca II emission strength or the greater difficulty in measuring Ca II emission among faint, cool stars characterized by complex molecular band spectra.

We emphasize that definite conclusions regarding either disk frequency or accretion properties based on the Ca II lines await both a better understanding of the contrast effects and higher spectral resolution studies capable of separating photospheric absorption, narrow-component emission, and broad-component emission. However, the apparently high frequency of Ca II emission sources amongst stars in our (randomly chosen) ONC spectroscopic sample suggests that accretion disks are prevalent.

7.3. *The Silhouette Disks and Externally Ionized Sources*

Among the most compelling lines of evidence for the existence of circumstellar disks around young stellar objects comes from the direct imaging of several objects in the ONC (McCaughrean & O'Dell 1996) with dark, extended structures seen in silhouette against the bright background of the Orion Nebula. Of these six stars, three have spectral types in our database that yield masses of 0.2, 0.3, and 2.0 $M_\odot$ and ages of 1.0, 1.0, and 2.0 Myr. None of these three have obvious Ca II emission, but they do have near-infrared excesses of magnitude $\Delta(I_C-K) = 0.7$, 0.1, and 0.8 mag.

The "silhouette disks" are a subset of a much larger population of extended structures recently identified from optical emission line studies at Hα, [N II], and [O III] of the Trapezium Cluster (see O'Dell & Wong 1996 and references therein). Several of these objects had been previously identified from ground-based optical and radio studies (see Lacques & Vidal 1979; Garay, Moran, & Reid 1987; Churchwell et al. 1987; Felli et al. 1993). In total, there are currently 152 objects that are thought to have photoionized regions in their near-circumstellar environments. Based on the morphologies and surface brightness distributions of these $\sim$100–1000 AU structures, the sources of the ionizing radiation are thought to be the O- and early B-stars of the Trapezium that produce Lyman continuum photons (McCullough 1993); models including the interaction with the ambient radiation field of ionized material carried in stellar or disk winds from the sources themselves have also been postulated (Henney et al. 1996; Johnstone, Hollenbach, & Bally 1998). Of the 152 externally ionized sources, 99 have been identified with optically visible stellar objects, while another 14 have been identified with infrared stellar objects. From the sample of 99 optical stellar sources, 70 have V- and I_C-band photometry, and 59 have spectral types reported in Hillenbrand (1997).

We have investigated the stellar properties of the externally ionized subsample of our assembled ONC data set in order to determine how these objects might differ from the nonionized objects that copopulate the ONC. We consider the spatial distribution, extinction distribution, mass distribution, age distribution, spectral features, and infrared properties. We can use this subsample—a set of objects that are theoretically postulated to be accretion disk systems—to gauge our sensitivity to the detection of disks, and of accretion disks.

As noted by O'Dell et al., the externally ionized sources are found most frequently in the vicinity of θ^1C Ori and θ^2A Ori (the two most massive stars in the region) and less frequently with increasing distance away from the central cluster (although they *are* found over the entire extent of the region surveyed by O'Dell et al.). Not *every* source located within the range of projected radii populated by the externally ionized sources shows these features, although it may be the case that in three dimensions the nonionized sources are located outside of the Stromgren radius of the ionizing OB stars. Based on a comparison of histograms normalized to the total number of stars in each sample, the distribution of spectroscopic extinction toward the O'Dell sources does not appear to be significantly different from that characterizing the overall ONC population, although there is some evidence for slightly higher extinction values. Likewise, the age distribution of the O'Dell sources does not appear different from that characterizing the overall ONC population. The mass distribution, however, may differ. Histograms normalized to the total number of stars in each sample (see Fig. 16*c*) show that (1) at high masses, the mass distribution of the O'Dell sources is no different from that characterizing the overall ONC population; in particular, there are a number of "early type" (G and early K) stars among the sources on the O'Dell lists, with masses of 1–3 $M_\odot$, and (2) at low masses, the same trend as was indicated in the comparison of stars with and without evidence for near-infrared excesses and Ca II triplet emission is found: the externally ionized sources are underrepresented at the lowest masses.

In the infrared, it appears based on the $\Delta(I_C-K)$ index that the O'Dell sample also does not differ from the overall population located within the same range of projected radii in terms of the fraction of infrared excess sources (about 80% for both samples). What is interesting, however, is that not *all* of the O'Dell sources have obvious evidence for circumstellar disks/envelopes. Analysis of $(J-H)$-$(H-K)$ colors leads us to the same conclusion. In raw color-color diagrams [$(V-I_C)$-(I_C-K) and $(J-H)$-$(H-K)$], the O'Dell sources appear to be somewhat redder than the overall stellar population. As it is unlikely that the increased reddening is due to their being more deeply embedded in the background molecular cloud, it may indicate a more significant contribution from extended circumstellar envelopes as opposed to compact disks. The O'Dell sources show a slightly higher incidence of broad Ca II triplet emission (about 50% frequency compared with about 40% for the overall population located over the same radial range). That the detection frequency of near-infrared excess and of Ca II emission is the same for this "proplyd" sample as for the general ONC population suggests that the general ONC population may have the same disk frequency as the "proplyd" sample: 100%!

We conclude that while their extended appearance in optical emission-line images distinguishes the O'Dell sources from the rest of the ONC stellar population, in general the stellar components of these sources are no different from "normal" young stars of low and intermediate mass and, in particular, are not different from their nonionized counterparts in the ONC. The O'Dell sources are slightly overrepresented among the objects with Ca II triplet emission and infrared excesses, but not *all* of the O'Dell sources have such evidence for the activity associated with circumstellar disks. There is weak evidence that the O'Dell

sources may be slightly more extincted on average than the rest of the ONC stellar population, which we postulate may be due to the more significant contribution of extended envelopes to the observed colors. In summary, the only distinguishing feature of these objects may be their current proximity to the ionizing radiation field of θ^1C Ori and θ^2A Ori as they pass on perigee through the inner part of the cluster.

8. CONCLUDING REMARKS

In this contribution, we have combined near-infrared photometry with optical photometry and spectroscopy in the ONC to study the frequency of circumstellar disks for a sample of stars with ages less than 0.1–2 Myr and masses <0.1–$50\ M_\odot$. We have defined an index, $\Delta(I_C-K)$, which quantifies the magnitude of the K-band excess above the photospheric level. We have discussed the errors associated with this index (Table 2) and considered them in our analysis. Stars in our sample show systematic trends with stellar mass and radius in the measured values of $\Delta(I_C-K)$: the index decreases toward stars of smaller mass and larger radius. These patterns are in qualitative agreement with model calculations (§ 3.2), which predict that the magnitude of the near-infrared excess should vary systematically with the properties of the central star according to changes in the contrast between photospheric and disk emission. Near-infrared excesses are expected to increase in magnitude with increasing stellar mass, decreasing stellar radius, increasing accretion rate, decreasing inner disk hole size, and decreasing inclination angle, although specific combinations of these parameters can produce results that deviate from the general trends. Quantitative comparison of the measured $\Delta(I_C-K)$ values with model expectations enables estimates of both the disk frequency and the disk accretion rates as a function of mass, age and position within the ONC.

Averaged over all stellar ages, stellar masses, and projected cluster radii represented by our ONC sample, disks still surround 55%–90% of the population. Independent evidence based on the Ca II triplet ($\lambda\lambda$8498, 8542, and 8662) seen either in emission or, at our spectral resolution, as "filled-in" absorption, suggests a disk fraction of $\sim$70%. We have also explored the evidence for trends in the disk frequency with stellar age, stellar mass, and projected cluster radius. We find no trend with stellar age, at least not over the limited age range ($\bar{\tau} < 1$ Myr) of stars in the ONC. We do, however, find variations in the disk frequency with stellar mass and with projected cluster radius (see Table 3).

Stars with masses $\gtrsim 3\ M_\odot$ have a significantly lower disk frequency than stars in the mass range $\sim$0.2–1.0 $M_\odot$, while stars with masses $\gtrsim 10\ M_\odot$ show no evidence for optically thick disks. These results suggest that the duration of the accretion disk phase is shorter (<1 Myr) among stars of intermediate and high masses than among stars of lower mass. The frequency of disk detection among the lowest mass ($\lesssim 0.2\ M_\odot$) stars may be lower as well. While the robustness of this result may be compromised by uncertainties in the modeling of both disk and photospheric colors at extremely low masses, analysis of the distribution of stellar masses among stars that show evidence of Ca II emission or externally ionized structures provides independent evidence of a lower disk frequency for objects with $M < 0.2\ M_\odot$. As this is only a 2–3 σ result (see Fig. 16), further study based on measurements at longer near-infrared wavelengths is required in order make definitive conclusions regarding disk frequencies among very low-mass stars.

Stars located in the inner regions (especially the inner 0.5 pc) of the cluster appear to have a higher disk frequency than stars located in the outer parts of the cluster. This finding has no explanation in terms of selection effects or photosphere/disk contrast issues. We speculate that this trend may be driven by differences in disk accretion properties. In particular, we suggest that stellar density, which increases toward the cluster center approximately as $\rho \propto r^{-2}$, may play some role. At $r \lesssim 0.3$ pc, where the mean separation between stars is only a few thousand AU, close encounters may result in tidally driven increases in $\dot{M}_{acc}$ (Ostriker 1994). However, other factors such as the role of the UV radiation field and/or stellar winds emanating from the central O stars in affecting the structure of the disks, and thus possibly the magnitude of the near-infrared excesses, must be considered.

The observed trends in disk frequency with stellar mass and projected cluster radius probably reflect some *combination* of the true frequency of stars surrounded by circumstellar disks and the relative importance of disk accretion. Many stars in our sample exhibit values of $\Delta(I_C-K)$ in excess of those expected from purely irradiative heating of the disks by their central stars. These are candidate accretion disk systems. From analysis of the ability of our $\Delta(I_C-K)$ diagnostic to select stars in the Taurus-Auriga dark cloud known to be accretion disk systems from ultraviolet excess measurements, we find that at least 34%–50% of our total ONC sample and at least 61%–88% of the disked sample are accretion disk systems.

We also wish to emphasize several points that may prove useful in guiding future studies of disk properties in star-forming regions or in reconsidering results from previously published work:

1. Estimating the fraction of stars surrounded by circumstellar disks from near-infrared excess emission requires considerable care, since the magnitude of the observed excess depends on a large number of variables: (*a*) stellar parameters (temperature/mass, radius/age), (*b*) disk parameters (accretion rate, inner disk hole size), (*c*) geometrical factors (inclination of the star/disk system), and perhaps even (*d*) environmental factors (e.g., location in a region characterized by high stellar density). Calculating disk fractions simply by counting the relative number of stars outside of and inside of reddening vectors in observed color-color diagrams without regard to these complicating effects is clearly naive (see the Appendix).

2. Near-infrared excesses (at J, H, and K band), to date the predominant means of judging whether a given star is surrounded by a disk, are particularly susceptible to the aforementioned effects. Measurements at L band are far less sensitive to these effects and would thus provide more robust estimates of disk frequencies among both optically visible and optically obscured young stellar populations. Only 43 stars in our sample of $\sim$1600 optically visible ONC stars have published photometry at L band!

3. Near-infrared excesses enable the detection of circumstellar disks only for star/disk systems characterized by $\dot{M}_{acc}$ values sufficient to heat the disk well above the temperatures imposed by radiative heating from the central star. While for higher mass star/disk systems even completely passive disks are detectable from observations at

near-infrared wavelengths, lower mass star/disk systems require higher accretion rates to drive an infrared excess. Such low-mass systems are probably more easily identified from ultraviolet excesses where the star/disk contrast is higher.

We thank J. Carpenter for insightful comments on a draft of this manuscript and an anonymous referee for a careful review of our work. Support to L. A. H. for this work was provided by NASA through grant HF1060.01-94A from the Space Telescope Science Institute, which is operated by the Association of Universities for Research in Astronomy, Inc., under NASA contract NAS5-26555. Publication of this work was supported by a grant to L. A. H. from NASA administered by the American Astronomical Society and from NASA Origins of Solar Systems grant NAG 5-7501. Support to N. C. was provided by NASA grants NAGW-2306 and NAG5-4282.

APPENDIX

EFFICIENCY OF DISK DETECTION FROM REDDENED COLOR-COLOR DIAGRAMS

In the main text we took advantage of a composite optical/infrared data set that included (1) optical photometry, (2) optical spectroscopy (enabling stellar mass and age estimates from the HR diagram), and (3) near-infrared photometry, in order to study the properties of circumstellar disks associated with stars in the ONC. We were able to correct the infrared photometry for the effects of interstellar/circumstellar extinction and for the underlying stellar photosphere to derive intrinsic I_C-K color excesses [$\Delta(I_C-K)$]. In this appendix we reconsider our entire photometric data set in light of our findings based on the subsample with optical spectroscopy. We ask how we can detect and study circumstellar disks in the absence of full photometric and spectroscopic information, that is, if we had to rely on statistical analysis of the location of reddened stars of unknown spectral type in an observed optical-infrared or infrared-infrared color-color plane. In particular, we derive the efficiencies of various color-color diagrams in diagnosing the presence of circumstellar disks.

Definitive identification of accreting systems is accomplished via the observation of optical spectral veiling (indicative of accretion directly onto the star) and/or forbidden line emission (indicative of accretion-driven stellar or disk winds). In Taurus-Auriga, 100% of the stars with measured veiling, $r > 10^{-2}$, and with forbidden line emission also have intrinsic colors (different from intrinsic color excesses, but similar in concept given the narrow spectral type distribution represented by Taurus) $(H-K)_0 > 0.2$ mag (Edwards et al. 1993) and $(K-L)_0 > 0.3$ mag (Hartigan et al. 1995). Thus intrinsic near-infrared excess, which is a strong indicator of the presence of heated circumstellar material, does appear to indicate accretion disk activity. What fraction of the systems known to be accreting in Taurus can be detected simply from their location in observed optical-infrared color-color diagrams?

Several different color-color diagrams have been used in the literature to diagnose circumstellar disks associated with young stars: $R-I$ versus $H-K$, $J-H$ versus $H-K$, and $H-K$ versus $K-L$ among them. Each of these planes samples the shape of the spectral energy distribution of a young stellar object of given mass in a different manner. Furthermore, the effects of the physical processes producing any infrared excess move stars along different vectors in these diagrams according to their mass. The combination of the behavior with stellar mass and the behavior with accretion disk properties means that in comparison with reddening vectors, each of these color-color diagrams has an efficiency factor in detecting young stars surrounded by circumstellar disks. Furthermore, the efficiency factor is governed by the *distribution* of stellar masses and the *distribution* of disk properties.

To test the efficiencies of various color-color planes in selecting star + disk/envelope systems, we first use the sample of classical and weak T Tauri stars in Taurus from Strom et al. (1989) and the sample of Herbig Ae/Be stars from Hillenbrand et al. (1992). Considering first the reddened $(V-I_C)$-(I_C-K) diagram, all T Tauri stars and all Herbig Ae/Be stars that do not have significant near-infrared emission from circumstellar gas and dust (i.e., weak T Tauri stars and Group III Herbig Ae/Be stars) lie within the regime populated by reddened stars with normal main-sequence colors. However, some of the classical T Tauri stars also have colors in this diagram that are consistent with reddened main-sequence stars. In other words, only some fraction of the stars with spectroscopic accretion signatures and intrinsic infrared excesses can be identified unambiguously as having continuum excess emission from the $(V-I_C)$-(I_C-K) diagram. Allowing for errors (and enforcing consistency with general practice in the literature), we count only those stars that lie ≥ 0.1 mag outside the reddening vector as having infrared excesses. By counting these as a fraction of the total number in the sample, we find the efficiency of the $(V-I_C)$-(I_C-K) diagram in detecting young stars analogous to classical T Tauri stars and Group I and Group II Herbig Ae/Be stars to be 68%. For comparison, the efficiency of the reddened $(V-I_C)$-$(H-K)$ plane is 70%, the efficiency of the reddened (R_C-I_C)-$(H-K)$ plane is 68%, and the efficiency of the reddened $(J-H)$-$(H-K)$ plane is 60%. Moving to the reddened $(H-K)$-$(K-L)$ diagram increases the fraction of infrared-identifiable objects with spectroscopic accretion signatures to 100%. In summary, while color-color diagrams allow us to pick out *most* of the Taurus-like and Herbig Ae/Be-like objects with circumstellar material, the disk/envelope frequencies *may* be 30%–40% higher than those derived by assuming that only objects lying completely outside of the reddening vectors have disks. The exception is when $K-L$ colors are available; an index that uses $K-L$ seems to pick out *all* candidate accretion disk systems, as was noted previously in the literature.

What about stars in the ONC? The efficiencies quoted above apply for the mix of spectral types, the extinction range, and the disk properties (accretion rates and inner disk hole sizes) characteristic of stars in the Taurus dark cloud. As shown in Hillenbrand (1997), the Orion database contains a higher fraction of later type stars compared with the Taurus database, with a mean spectral type in the ONC of M3–M4 versus a mean spectral type in Taurus of K7–M0. Because stars of later spectral type need a larger infrared excess to make them unambiguously distinguishable from reddened earlier type stars, the so-called efficiency factors calculated above may not apply.

We can test this assertion by comparing the fraction of stars identified as having disks from our $\Delta(I_C-K)$ index with the fraction identified from the reddened $(V-I_C)$-(I_C-K), $(V-I_C)$-$(H-K)$, and $(J-H)$-$(H-K)$ diagrams (Figs. 2, 3, and 4). From the $(V-I_C)$-(I_C-K) diagram, of the 1114 ONC sources with V-, I-, and K-band photometry, 336 or 30% lie more than 0.1 mag above the reddening vectors drawn from the dwarf/giant sequence. From the $\Delta(I_C-K)$ index we found 64% of the 813 stars in this diagram with determined spectral types to have more than 0.1 mag of intrinsic excess. For a distribution of spectral types like that in the ONC, therefore, the efficiency of the $(V-I_C)$-(I_C-K) diagram seems more like 47% than the 68% found from Taurus. Similarly, from the $(J-H)$-$(H-K)$ diagram, of the 1101 optically visible ONC sources with J-, H-, and K-band photometry, 217 or only 20% lie more than 0.1 mag to the right of the reddened dwarf/giant sequence. Thus for a distribution of spectral types like that in the ONC, the efficiency of the $(J-H)$-$(H-K)$ diagram seems more like 31% instead of the 60% found from Taurus. The $(J-H)$-$(H-K)$ diagram is less efficient than the $(V-I_C)$-(I_C-K) diagram in picking out objects with near-infrared continuum excess because of the less-distinguishable behavior in the $(J-H)$-$(H-K)$ plane of reddening and excess emission from heated gas and dust, particularly in late-type systems where the temperatures of the inner circumstellar material are comparable with those of the central stars. The $(J-H)$-$(H-K)$ diagram appears useful for diagnosing only rapidly accreting low-mass star/disk/envelope systems, but both active and passive high-mass star/disk/envelope systems.

In summary, the utility of a given color-color diagram in correctly assessing the frequency of near-infrared excess emission depends on the distribution of all of the same parameters discussed in the main text for diagnosing circumstellar disks from an intrinsic color excess: stellar mass, stellar radius, disk accretion rate, disk inclination, and inner disk hole size. An observed color-color diagram, however, has the added feature of susceptibility to the distribution of extinction properties in combination/competition with the distribution of stellar and disk properties. Simply counting the fraction of stars that lie inside and outside of reddening vectors in an observed color-color diagram to derive the disk frequency can be quite misleading. This practice does, however, always yield a lower limit to the disk frequency. We found an efficiency of $\sim 50\%$ for the $(V-I_C)$-(I_C-K) diagram and $\sim 30\%$ for the $(J-H)$-$(H-K)$ diagram in picking out stars with infrared excess, for a distribution of stellar masses, stellar ages, circumstellar disk properties, and extinction properties similar to ONC stars. These efficiencies are lower than found for star/disk systems in Taurus.

REFERENCES

Ali, B., & DePoy, D. L. 1995, AJ, 110, 2415
Allen, L. E. 1996, Ph.D. thesis, Univ. Massachusetts
Basri, G., & Bathala, C. 1990, ApJ, 363, 654
Batalha, C. C., Stout-Batalha, N. M., Basri, G., & Terra, M. A. O. 1996, ApJS, 103, 211
Breger, M., Gehrz, R. D., & Hackwell, J. A. 1981, ApJ, 248, 963
Calvet, N., et al. 1999, in preparation
Calvet, N., Magris, G. C., Patino, A., & D'Alessio, P. 1992, Rev. Mexicana Astron. Astrofis., 24, 27
Calvet, N., Patino, A., Magris, G. C., & D'Alessio, P. 1991, ApJ, 380, 617
Choi, P. I., & Herbst, W. 1996, AJ, 111, 283
Churchwell, E., Felli, M., Wood, DoS., & Massi, M. 1987, ApJ, 321, 516
D'Antona, F., & Mazzitelli, I. 1994, ApJ, 90, 467
Edwards, S., et al. 1993, AJ, 106, 372
Edwards, S., Hartigan, P., Ghandour, L., & Andrulis, C. 1994, AJ, 108, 1056
Elias, J. H., Frogel, J. A., Matthews, K., & Neugebauer, G. 1982, AJ, 87, 1029
Ellis, T., Drake, R., Fowler, A. M., Gatley, I., Heim, J., Luce, R., Merrill, K. M., Probst, R., & Buchholz, N. 1992, Proc. SPIE, 1765, 94
Felli, M., Churchwell, E., Wilson, T., & Taylor, G. B. 1993, A&AS, 98, 137
Garay, G., Moran, J. M., & Reid, M. J. 1987, ApJ, 314, 535
Genzel, R., Reid, M. J., Moran, J. M., & Downes, D. 1981, ApJ, 224, 884
Gillett, F. C., & Joyce, R. R. 1975, BAAS, 7, 409
Gullbring, E., Hartmann, L., Briceño, C., & Calvet, N. 1998, ApJ, 492, 323
Hamann, F., & Persson, S. E. 1992, ApJS, 82, 247
Hartigan, P., Edwards, S., & Ghandour, L. 1995, ApJ, 452, 736
Hartigan, P., Kenyon, S. J., Hartmann, L., Strom, S. E., Edwards, S., Welty, A., & Stauffer, J. 1991, ApJ, 382, 617
Hartmann, L., Calvet, N., Gullbring, E., & D'Alessio, P. 1998, ApJ, 495, 385
Hartmann, L., Hewett, R., & Calvet, N. 1994, ApJ, 426, 669
Henney, W. J., Raga, A. C., Lizano, S., & Curiel, S. 1996, ApJ, 465, 216
Herbig, G. H., & Soderblom, D. R. 1980, ApJ, 242, 628
Herbig, G. H., & Terndrup. 1986, ApJ, 307, 609
Hillenbrand, L. A. 1997, AJ, 113, 1733
Hillenbrand, L. A., et al. 1999, in preparation
Hillenbrand, L. A., & Hartmann, L. W. 1998, ApJ, 492, 540
Hillenbrand, L. A., Massey, P., Strom, S. E., & Merrill, K. M. 1993, AJ, 106, 1906
Hillenbrand, L. A., Meyer, M. R., Strom, S. E., & Skrutskie, M. F. 1995, AJ, 109, 280
Hillenbrand, L. A., Strom, S. E., Vrba, F. J., & Keene, J. 1992, ApJ, 397, 613
Hollenbach, D., Johnstone, D., Lizano, S., & Shu, F. 1994, ApJ, 428, 654
Jarrett, T. H. 1992, Ph.D. thesis, Univ. Massachusetts
Johnstone, D., Hollenbach, D., & Bally, J. 1998, ApJ, 499, 758
Jones, T. J., Mergen, J., Odewahn, S., Gehrz, R. D., Gatley, I., Merrill, K. M., Probst, R., & Woodward, C. E. 1994, AJ, 107, 2120
Joyce, R. R., Hinkle, K., Meyer, M. R., & Skrutskie, M. F. 1998, Proc. SPIE, 3354, in press
Kenyon, S. J. 1988, AJ, 96, 337
Kenyon, S. J., & Hartmann, L. 1995, ApJS, 101, 117
Lacques, P., & Vidal, J. L. 1979, A&A, 73, 97
Lee, T. A. 1968, ApJ, 152, 913
McCaughrean, M. J., & O'Dell, C. R. 1996, AJ, 111, 1977
McCaughrean, M. J., & Stauffer, J. R. 1994, AJ, 108, 1382
McCullough, P. R. 1993, Ph.D. thesis, Univ. California, Berkeley
McNamara, B. J. 1976, AJ, 81, 845
Meyer, M. R., Calvet, N., & Hillenbrand, L. A. 1997, AJ, 114, 288
Muzerolle, J., Calvet, N., & Hartmann, L. 1998, ApJ, 492, 743
Ney, E. P., Strecker, D. W., & Gehrz, R. D. 1973, ApJ, 180, 809
Penston, M. V. 1973, ApJ, 183, 505
Penston, M. V., Hunter, J. K., & O'Neill, A. 1975, MNRAS, 171, 219
O'Dell, C. R., & Wong, K. 1996, AJ, 111, 846
Ostriker, E. C. 1994, ApJ, 424, 292
Rydgren, A. E., & Vrba, F. J. 1984, AJ, 89, 399
Samuel, A. E. 1993, Ph.D. thesis, Australian National Univ.
Shu, F., Najita, J., Ostriker, E., Wilkin, F., Ruden, S., & Lizano, S. 1994, ApJ, 429, 781
Skrutskie, M. F., Dutkevitch, D., Strom, S. E., Edwards, S., Strom, K. M., & Shure, M. A. 1990, AJ, 99, 1187
Smith, J. R. 1976, Ph.D. thesis, Univ. Wyoming
Strom, K. M., Strom, S. E., Edwards, S., Cabrit, S., & Skrutskie, M. F. 1989, AJ, 97, 1451
Valenti, J. A., Basri, G., & Johns, C. M. 1993, AJ, 106, 2024
Walker, M. F. 1969, ApJ, 155, 447